Chapter 12
Intrafolial folds: Review and examples from the western Indian Higher Himalaya

SOUMYAJIT MUKHERJEE[1], JAHNAVI NARAYAN PUNEKAR[2], TANUSHREE MAHADANI[1], and RUPSA MUKHERJEE[1]

[1] *Department of Earth Sciences, Indian Institute of Technology Bombay, Powai, Mumbai 400076, Maharashtra, India*
[2] *Department of Geosciences, Princeton University, Princeton, NJ, USA*

12.1 INTRODUCTION

Folds are perhaps the most intensively studied structures in geology (for example Ramsay 1967; Ez 2000; Harris et al. 2002, 2003, 2012a,b; Alsop and Holdsworth 2004; Mandal et al. 2004; Carreras et al. 2005; Bell 2010; Hudleston and Treagus 2010; Godin et al. 2011). Depending on morphologies and orientations, folds can be classified using several schemes (reviews by Ghosh 1993; Davis et al. 2012, etc.). Besides their rheological aspects, deciphering whether folds inside any shear zones are produced by shear has been emphasized (e.g. Mandal et al. 2004; Carreras et al. 2005; Bell et al. 2010). A couple of shear zone models altogether neglected fold formation within them, for example Koyi et al. (2013), Mukherjee and Biswas (this volume, Chapter 5), Mulchrone and Mukherjee (in press). Mukherjee (2012a, 2014a) investigated the issue in terms of deformation of inactive markers in inclined shear zones undergoing extrusion and subduction. Folds related to shear zones are broadly of two types: (i) those with low interlimb angles and with significantly curved hinge lines developed before shear, some of which are sheath folds; and (ii) flow perturbed syn-shear folds that may be overturned and "intrafolial" (Alsop and Holdsworth 2004). In shear zones, locally overturned isoclinally folded foliations bound by straight foliation planes are most commonly called "intrafolial folds" (*intra* = inside; *folia* = foliation) (Dennis 1987; Allaby 2013). Intrafolial folds are found most commonly in mylonites (Trouw et al. 2000). Such folds have also been reported from cataclasites and obsidian (Higgins 1971), deformed soft sediments (Jirsa and Green 2011), slump structures (Woodcock 1976) and debris flows (Gawthrope and Clemmey 1985). The vergence of these folds is in conformity with shear sense of the shear zones they occur in. Intrafolial folds are disrupted to rootless folds if shear is more intense than in the adjacent layers even on a local scale. The adjacent rocks might be undeformed as well (Neuendorf et al. 2005). These folds tightened as shear continued (Longridge et al. 2011). Early references to classical intrafolial folds as "drag folds" (e.g. fig. IX-38 in Hills 1965) were subsequently not followed. Carrerras et al. (2007) viewed intrafolial folds both as "syn-shear folds", and "shear-related late folds" (their fig. 1c). Depending on other mechanisms perceived for intrafolial folds, they have also been described as "intrafolial strain-slip folds" (Ratcliffe and Harwood 1975) and "intrafolial shear folds" (Keiter et al. 2011). Intrafolial folds can tear apart by pronounced shear into rootless folds showing opposite closure (as in fig. 4.6B of Park 1997). Intrafolial folds have been referred to mainly as byproducts of some other studies, either as one of the ductile shear sense indicators in the field (Gangopadhyay 1995 but also others) or thin-sections (Trouw et al. 2010); or for their progressive evolution and geneses. Most of these were deduced on field observations (e.g. Passchier et al. 1991), with very few analytical- (Hara and Shimamoto 1984) and analog models (Bons and Jessel 1998). Notice that well before the concept of ductile shear dominated structural geology literature, intrafolial folds were explained in the same way in terms of "fluxion plane" and "fluxion layers" (Higgins 1971). Studying intrafolial folds is of practical importance, since a few ore bodies have been deciphered to be intrafolially folded (e.g. Laznicka 1985).

This chapter reviews morphologies and geneses of intrafolial folds. We also discuss use of such folds to determine shear senses from particular Himalayan shear zones.

12.2 GEOLOGY AND TECTONICS OF THE STUDY AREAS

The Higher Himalayan Shear Zone (HHSZ) consists of gneisses and schists of Precambrian and Proterozoic ages at dominantly greenschist to amphibolite facies (Grasemann et al. 1999; Grasemann and Vannay, 1999; Vannay et al. 1999; Vannay and Grasemann 2001;

Ductile Shear Zones: From Micro- to Macro-scales, First Edition. Edited by Soumyajit Mukherjee and Kieran F. Mulchrone.

Jain et al. 2005; Mukherjee, in press). The southern margin of the HHSZ is the "Main Central Thrust" (MCT = Main Central Thrust-Lower: MCT_L of Godin et al. 2006) and the northern boundary the South Tibetan Detachment System (or the South Tibetan Detachment System-Upper: $STDS_U$ of Godin et al. 2006). The lower boundary of the HHSZ is now conventionally viewed as the MCT-zone, which is a mixture of Higher Himalayan and the underlying Lesser Himalayan rocks. The northern boundary of this zone is designated as the MCT-Upper (MCT_U) (review by Godin et al. 2006). The HHSZ is characterized by pre-Himalayan D_1 folding, a D_2 top-to-S/SW ductile shear, and post-Himalayan D_3 folding (review by Jain et al. 2002). Throughout the HHSZ, the D_2 phase of top-to-S/SW ductile shear was documented where N/NE dipping "main foliations" acted as the primary shear C-planes. In addition, a late top-to-NE ductile shear developed inside the $STDS_U$ along the same NE dipping main foliations (Burchfiel et al. 1992; Godin et al. 2006). Inside the HHSZ, one more ductile shear zone with normal shear sense – the South Tibetan Detachment System Lower ($STDS_L$) was delineated from both the eastern (review by Godin et al. 2006) and the western Himalaya (Mukherjee and Koyi 2010a). The $STDS_U$ and the $STDS_L$ are spatially separated. The timing and the magnitude of slip of the tectonic boundaries/zones- the MCT, the $STDS_U$ and the $STDS_L$ varies along the entire Himalayan chain. Slip of the $STDS_U$ varies from 42–255 km along the Himalayan chain (review by Leloup et al. 2010). In general, the timing of extensional shear within the $STDS_U$ was ~19–94 Ma, and the $STDS_L$ was ~24–42 Ma (Godin et al. 2006; Yin 2006). The extensional shear of the $STDS_U$ stopped ~5 Ma earlier in the western than in the eastern Himalaya (Leloup et al. 2010). Unlike the previously held view that the STDS developed by continuous deformation of a low-angle normal fault system, its genesis is now linked to both channel flow and extrusion (Kellett and Grujic 2012; also see Mukherjee 2005).

An inverted metamorphic gradient is indicated inside the HHSZ by isograds of high-grade minerals at the base (that is in the S), and considerable melting at or near the top (in the N). Three metamorphic episodes of the HHSZ have been deciphered: local M_1 phase around granite plutons; prograde M_2 metamorphism during the top-to-SW shear, and finally M_3 retrogression (see review by Jain et al. 2002) during crustal unroofing. Alternately, HHSZ metamorphosed either in two events- in the Eo-Himalayan (>44 – 33 Ma) and the Neo-Himalayan periods (~18 Ma), or through a protracted single phase (reviewed by Yakymchuk and Godin 2012).

The HHSZ extruded initially by a top-to-SW shear (the D_2 phase) from ~25 Ma (Yin 2006). This was followed by a crustal channel flow along with a top-to-SW shear since ~18 Ma (Mukherjee 2005, 2009, 2012a,b, 2013a,b, 2014b, for reviews; Godin et al. 2006; Hodges 2006; Yin 2006; Harris 2007; Mukherjee and Koyi 2010a). The $STDS_U$ and the $STDS_L$ were considered to be produced during channel flow affecting different portions of the HHSZ (see Hollister and Grujic 2006; Mukherjee and Koyi 2010a for details). The relative role of tectonics and erosion in sustaining the channel flow is debated (reviews by Mukherjee 2005; Godin et al. 2006; Hodges 2006; Jones et al. 2006; Yin 2006; Harris 2007; Mukherjee and Koyi 2010a; Godard and Burbank 2011). A more recent postulate is that the HHSZ extruded by channel flow flip-flop alternating with intervals of critical taper mechanisms (Beaumont and Jamieson 2010; Chambers et al. 2011).

The $STDS_U$ is locally known as the Zanskar Shear Zone (ZSZ) in Kashmir (India). The ZSZ is a ~1 km thick zone of mylonites (Dèzes et al. 1999), has a throw of 15–50 km (Herren 1987), and exhibits normal way up metamorphic isograds (review by Walker et al. 2001). The ZSZ shows three dominant deformations: (i) a top-to-SW compressional shear, (ii) subsequent top-to-NE extensional shear, and (iii) a latest top-to-NE (down) extensional ductile shear (Herren 1987; Patel et al. 1993; Dèzes et al. 1999; Jain and Patel 1999; Mukherjee 2007, 2010b; Mukherjee and Koyi 2010b). The $STDS_L$ has not yet been reported from the Zanskar section.

In the Sutlej section (Himachal Pradesh, India), schists constitute the southern part of the HHSZ, and gneisses, migmatites and granites the upper part (Mukherjee and Koyi 2010a). A component of pure shear was quantified from this section as having a kinematic vorticity number of 0.86 (Grasemann et al. 1999), or 0.73–3.81 (Law et al. 2010). S to N, up to the MCT_U, the peak metamorphic temperature rose from 610 to 700°C and the peak pressure fell from 900 to 700 MPa (Vannay et al. 1999) indicating metamorphism at ~30 km depth (Vannay and Grasemann 2001).

This work documents intrafolial folds in the HHSZ of the Sutlej river section (Fig. 12.1a): both from inside and outside the $STDS_U$ and the $STDS_L$; and from the XZ oriented thin-sections of the ZSZ (Fig. 12.1b). Based on pre-existing geochronological data and a number of trial tectonic models, Mukherjee and Koyi (2010a) argued that in Sutlej section, the most plausible timing of extensional shear in the $STDS_U$ (normal shear sense) had a shorter span of ~15–54 Ma than ~14–42 Ma within the $STDS_L$. Godin et al. (2006) considered that the ZSZ underwent extensional shear during 18–86 Ma (data originally by Inger 1998). The intrafolial folds of the Zanskar Shear Zone underwent a top-to-N/NE ductile shear during the same time span (Mukherjee and Koyi 2010b; Mukherjee 2010b).

12.3 REVIEW OF INTRAFOLIAL FOLDS

12.3.1 Intrafolial folds *sensu stricto*

12.3.1.1 Morphologies

Where the intrafolial folds occur in trains, these folds approximate periodic asymmetric waves (Ramsay 1967) that are tight to isoclinal (Park 1997) with thick hinges and thin limbs. These folds seldom have straight limbs or sharp hinges. Most have curved limbs and round hinges

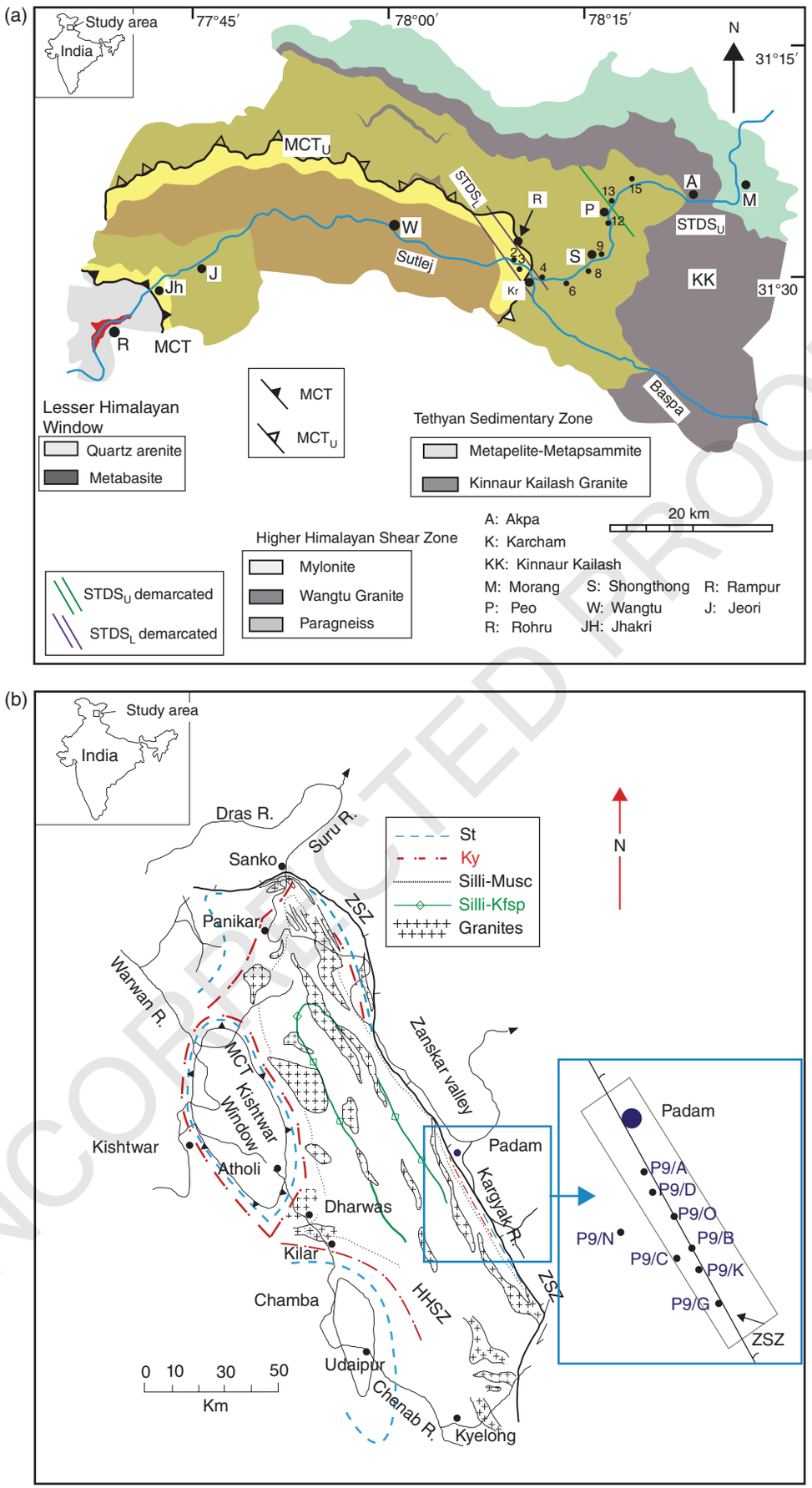

Fig. 12.1. The study areas. Numbers indicate sample locations. (a) Higher Himalayan Shear Zone, Sutlej river section (Singh, 1993; Srikantia and Bhargava, 1998; Vannay and Grasemann, 1998). The location of the "Main Central Thrust" (MCT) that bounds the Lesser Himalayan rocks is as per Singh (1993). The Vaikrita Thrust of Srikantia and Bhargava (1998) is designated as the "MCT-Upper" (MCT$_U$) of Godin et al. (2006). (b) Higher Himalayan Shear Zone, Zanskar section. Source: Searle et al. 1988. Reproduced with permission of The Royal Society.

in axial profiles. In single trains, one set of limbs is usually longer than the other. Such morphologies are also reported from intrafolial folds developed within debris flow (Gawthorpe and Clemmey 1985).

12.3.1.2 Genesis

Intrafolial folds can form in four ways: (i) folding a part of a foliation during shear along the later (Fig. 12.2a; from Passchier and Trouw 2005), or whole of the foliation planes (Winter 2012); (ii) modification of pre-existing structures/features, for example, cross-beddings and dykes; (iii) folding of foliations formed during simple shear; and (iv) remnant folded layers by flattening/unfolding that are more competent than the surrounding straight and completely unfolded layers (Llorens et al. 2013). For case (iii) above, the fold hinge rotated along with shear (Duebendorfer et al. 1990). For case (iv), the competent bed could be limestone where intrafolial folds are confined and are bound by incompetent shale dominated rock (Linn et al. 2002). Ez (2000) concluded that a shear perfectly parallel to the foliation plane cannot produce any folds. Such folds can be initiated by rotation of foliations around any harder inclusion (Fossen 2010). In other words, some hindrance to simple shear is needed for intrafolial folds to develop (Swanson 1999). However, a hindrance can also produce kinks and crenulations (Swanson 1999). He demonstrated how a pre-existing symmetric fold shears into an "overturned fold" (= folds with limbs of nearly the same dip direction). Limbs vary greatly in thickness on either side of a thick hinge (Fig. 12.2b; fig. 11.23 of Fossen 2010). Best (2006) proposed that simple shear of straight foliation

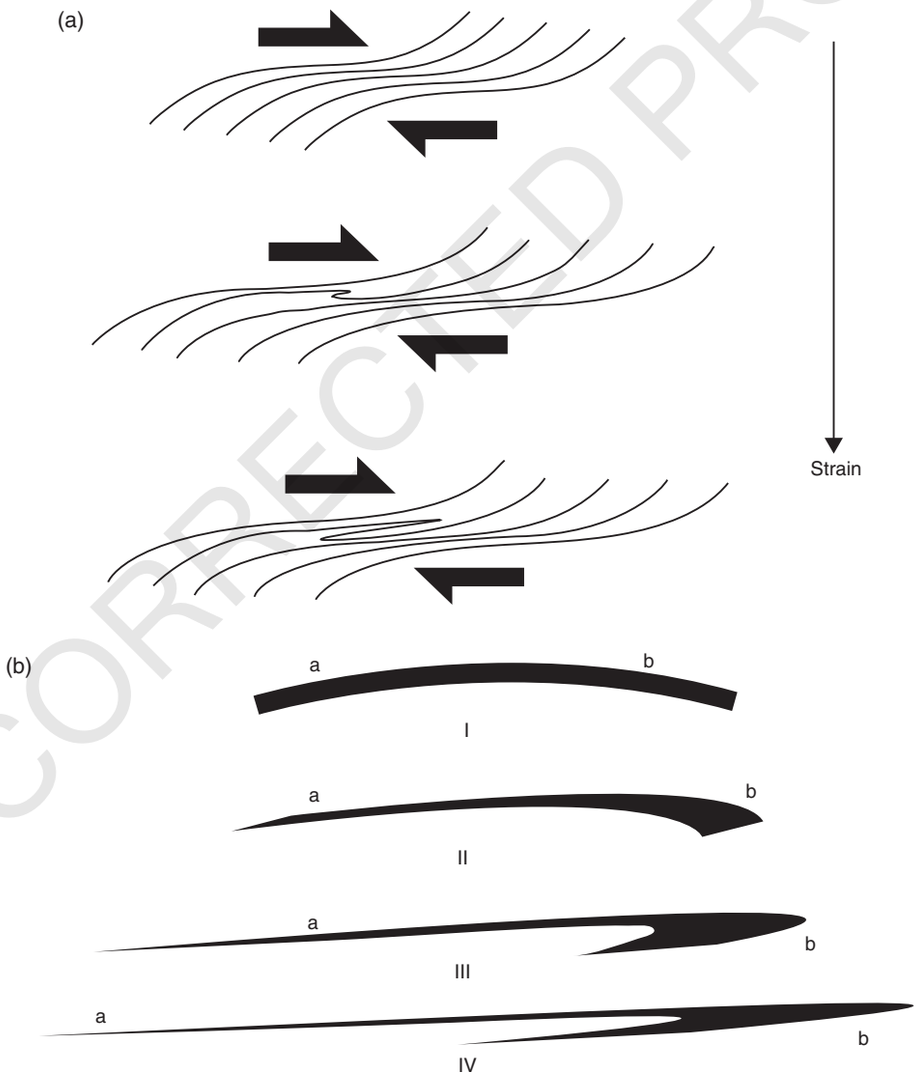

Fig. 12.2. (a) Ductile shear gives rise to intrafolial folds in a single shear event due to the presence of inhomogeneity in the rock. Source: Passchier and Trouw 2005. Reproduced with permission from Springer Science + Business Media. (b) A symmetric fold becomes asymmetric and overturned due to simple shear. The hinge is thickened and the two limbs vary in thickness and length. Source: Fossen 2010. Reproduced with permission of Cambridge University Press. Limbs 'a' and 'b' are marked and plotted in Ramsay's (1967) scheme in Fig. 12.16.

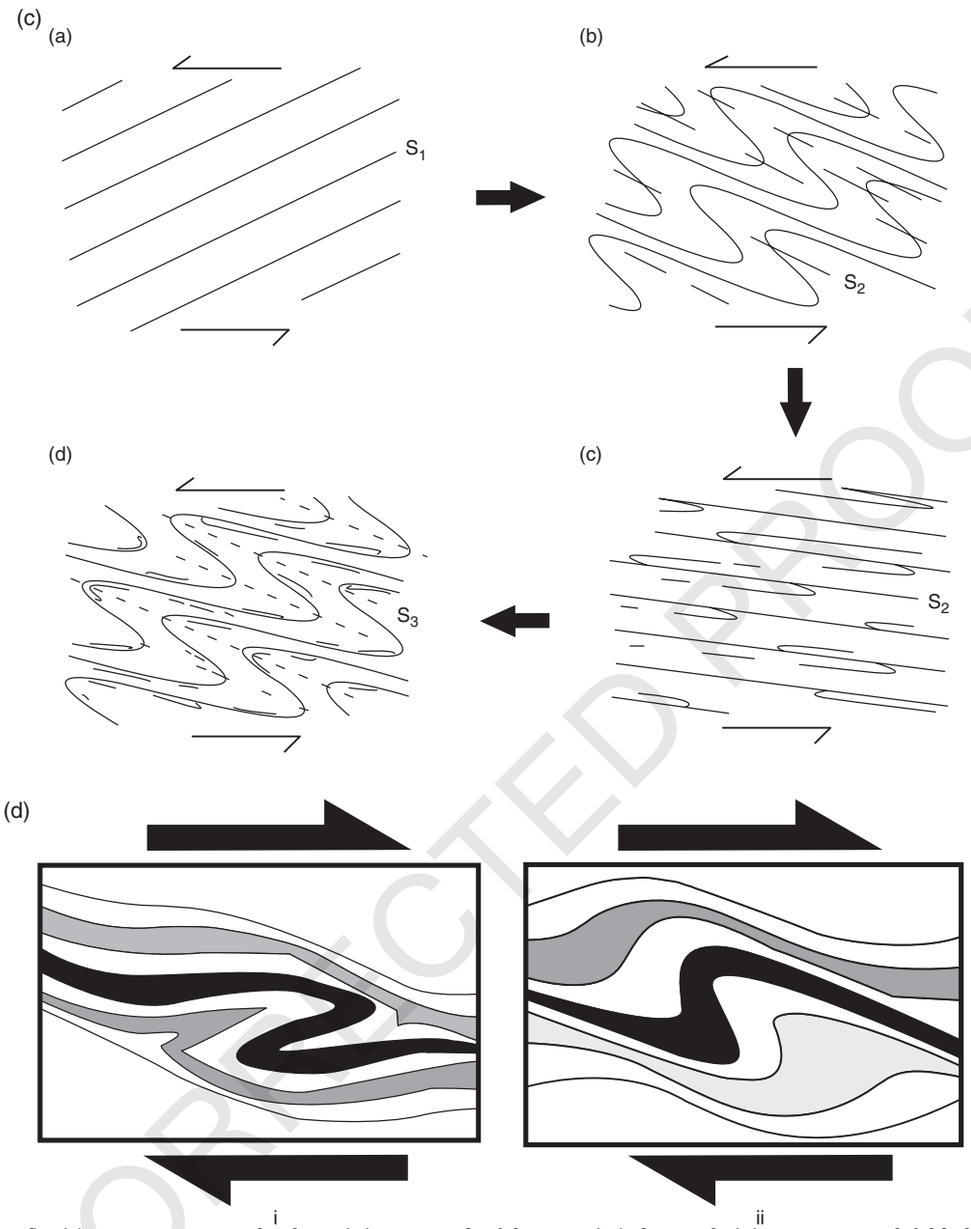

Fig. 12.2. (*Continued*) (c) Progressive simple shear (A) on straight foliations (S_0) depicted. (B) S_0 overturned folded and axial planar foliations (S_1) develop. (C) S_1 are slipped, where the S_2 act as brittle fault planes. (D) S_2 gets overturned folded and straight S_3 axial planar foliations develop. Source: Best 2006. Reproduced with permission of John Wiley & Sons. (d) i. Synthetic fold, ii. Antithetic or back-rotated fold produced by secondary shear associated with top-to-right shear. Source: Lebit et al. 2005. Reproduced with permission from Elsevier.

planes can develop progressively overturned folds on a number of subsequent foliation planes (Fig. 12.2c). Shear magnifies initial curvatures of planar markers and their hinges to develop intrafolial folds (fig. 3.21a of Passchier et al. 1991). Taking a mixture of octachloropropane and camphor as the model material in a Taylor–Couette flow with the shear strain varying from 111 to 122, Bons and Jessel (1998) modeled development of intrafolial folds in a train. Initial irregularities evolved into fold hinges as the pre-developed fold axes attained gentler plunges.

The common perception of a fold inside an apparently undeformed matrix is that the folded material is of much lower viscosity than the matrix (fig. 3–34 of Billings 2008; also Nevin 1957). Ez (2000) questioned whether straight foliations that bound intrafolial folds are really undeformed zones. Any (competent) quartzite or pegmatite vein within a schistose rock-mass can also facilitate the competence difference and develop intrafolial folds (Harris et al. 2002). However, Whitten (1966) referred (in his fig. 175) to a number of intrafolial folds in marbles where the folded material and the matrix appear to be composed of the same mineral. Hara and Shimamoto (1984) inferred from such examples that viscosity contrast between the fold and the

matrix does not seem to be a significant genetic factor for such folds. This conjecture is also found in the postulation of Carrerras et al. (2005) that these folds develop from an isotropic unfoliated rock body by ductile shear, whereby foliations form and fold simultaneously at local scales.

The disparity in thickness between different parts of a single fold becomes more acute with progressive deformation. This indicates that as shearing proceeds, materials flow from both limbs towards the hinges attenuating the limbs until they break (also fig. 3-30 of Ramsay, 1967). The limbs and axial planes are usually at low-angles to foliations that are regionally straight. Extreme shear may lead to tearing of the fold trains into disconnected folds of same overall geometry and orientation (fig. 4.19 of Passchier et al. 1991). On the other hand, shear can reduce the angle between the axial plane and the regional foliation so that they sub-parallel (fig. 12.27 of van der Pluijm and Marshak 2004). In this case, the sense of shear becomes indistinct. However, continued shear can redevelop an intrafolial fold with the previous folded fabric preserved within it (fig. 12.27c of van der Pluijm and Marshak 2004).

12.3.1.3 Shear sense

Passchier and Trouw (2005) cautioned that unless the three-dimensional shapes of the folds before they became intrafolial are known, and unless the plane of observation perpendiculars the main foliation and parallels stretching lineation, intrafolial folds are not reliable shear sense indicators (also see Fossen 2010). However, whereas the second constraint of selecting the proper plane was used to deduce shear senses in the field- and thin-sections (e.g. Mukherjee 2007, 2010a,b, 2011a; Mukherjee and Koyi 2010a,b), the first condition was not considered since the ductile shear sense indicated by those folds matched well with other shear sense indicators, most notably with mineral fish (Mukherjee 2011b) and sigmoidal quartz veins. Another point of caution is that Carrerras et al. (2007) documented back rotated folds due to ductile secondary shear. Though these folds resemble intrafolial folds, they indicate an opposed shear sense (Fig. 12.2d). Intrafolial folds are reliable ductile shear sense indicators if they are regionally common and if unassociated with any regional folds (Davis et al. 2012).

12.3.2 Intrafolial folds *sensu lato*

A number of other situations also give rise to intrafolial folds *sensu lato*. We call them *sensu lato* since these were not described so far as "intrafolial folds". For example, Harris et al. (2002) and Fossen (2010) demonstrated how a linear marker initially at a high angle to the shear direction reorients, shortens and folds to a "hook" shape (see Fig. 12.3a) showing an apparent ductile shear sense. An important observation from Fig. 12.3a is that the long limbs of such folds do not parallel the primary shear C-planes. Retro-shear on a sigmoid S-fabric (Fig. 12.3b; fig. 9 of Wennberg, 1996; also fig. 3a of Aller et al. 2011) also yields foliation bound hooks. Such hooks of leucosomes and quartz veins were documented in metasedimentary rocks on mesoscopic scales in other shear zones (figs. 6.38 and 6.44 of Vernon and Clarke 2008), and in mylonites on micro-scales (Mukherjee 2007; fig. 8 of Mukherjee and Koyi 2010b). At the two corners of microscopic quarter structures and symmetric phi-objects, the foliation planes locally attains overturned folds in accordance with the shear sense (Fig. 12.3c; fig. 15.33 of Bobyarchick, 1998; fig. 43B of Davis et al. 1998; fig. 15.33 of Fossen, 2010; figs. 9.7.9–9.7.12 of Trouw et al. 2010). Occasionally, one may encounter microscopic single mineral grains displaying intrafolial folds (Fig. 12.3d; figs. 7b,-c of ten Grotenhuis et al. 2003; same as fig. 5.32d Passchier and Trouw, 2005; and fig. 9.5.16 of Trouw et al. 2010; also folded garnet in Mukherjee, 2010a). In meso- and microscopic flanking structures, host fabric elements locally fold and drag near cross-cutting elements (Fig. 12.3e; figs. 2a-d of Mukherjee 2011; also see Becker 1995). While the cross-cutting element could be dykes, fractures, joints, faults, secondary shear planes or zones, veins, melt such as leucosomes, burrows, inclusions, minerals, or boudins; the host fabric element can be bedding planes, foliations, lineations, mineral cleavages, and grain margins (Mukherjee and Koyi. 2009, and references therein). Intrafolial parasitic folds also develop by ductile shear over first generation flexure slip folds (fig. 54 of Nevin, 1957). Parasitic S- and Z- shaped folds were considered intrafolial when they are bound by a pair of foliation planes (Maass et al. 1980). Where multiple generations of foliations survived, the n^{th} generation of straight foliation might cut across and confine the $(n-1)$ generation of folded foliation (Fig. 12.3f). These folded foliations need not be produced by ductile shear, and could merely be asymmetric folds (fig. 4 of Bell 2010). Compression (pure shear) perpendicular to foliations that are axial planar to symmetric folds transposes/crenulates folds bound by the newly formed foliation. This holds both for vertical and inclined axial planes of the initial folds (Davis et al. 2012; figs. 12.27a-c of van der Pluijm and Marshak 2004; fig. 12.22 of Fossen 2010). On pronounced compression, however, these folds straighten (fig. 4.18-b of Passchier and Trouw 2005). If the C-plane of simple shear are compressed orthogonally, the prior shear-induced foliations can develop intrafolial folds with a vergence perpendicular to the direction of the preceding shear (Fig. 12.3g; fig. 3.21a of Passchier et al. 1991).

12.4 PRESENT STUDY

12.4.1 Do the studied intrafolial folds fall into *sensu stricto*, or *sensu lato category*?

Quartz rich layers and/or leucosomes define some of the intrafolial folds in the Sutlej section. They occur in a train outside the two detachments, the $STDS_U$ and the $STDS_L$,

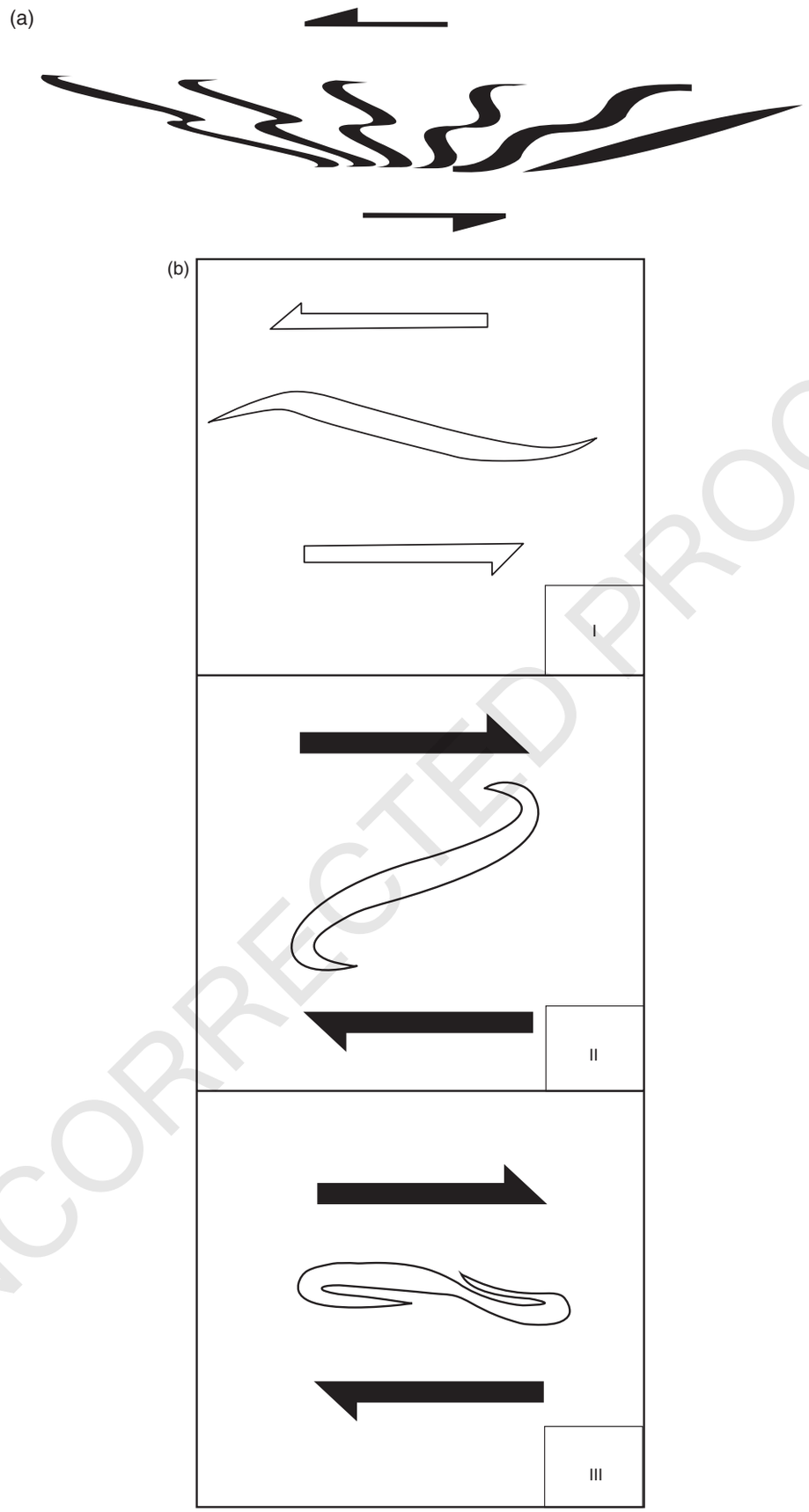

Fig. 12.3. (a) Top-to-left shear on a rightward inclined marker finally leads to intrafolial folds with longer limb dipping towards right and the shorter one towards left. Source: Fossen 2010. Reproduced with permission of Cambridge University Press; also see fig. 12.26 of van der Pluijm and Marshak 2004; fig. 7–72 of Ramsay 1967; fig. 1m of Harris 2003). (b) Reactivation of a top-to-left sheared fabric (I) into a later top-to-right one (II) leads ultimately to folded fabric at low angle to the plane of shear (III). Source: Wennberg, 1996. Reproduced with permission from Elsevier.

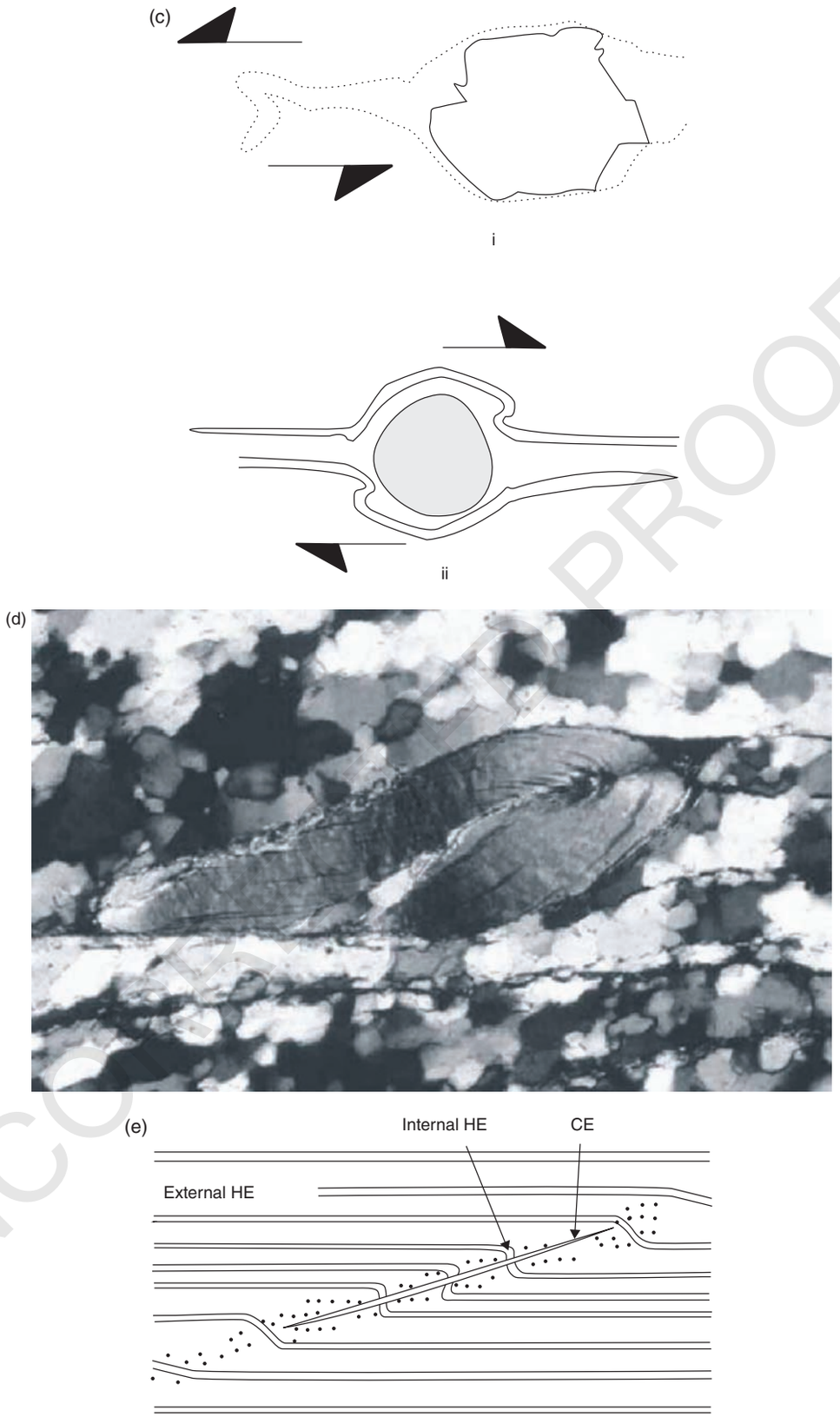

Fig. 12.3. (*Continued*) (c) A quarter structure where near the two corners of a clast, intrafolial folded foliation planes occur. Source: Passchier and Trouw 2005. Reproduced with permission from Springer Science + Business Media. (d) An isoclinally and intrafolial folded single grain of mica under microscope. Source: ten Grotenhuis et al. 2003. Reproduced with permission from Elsevier. (e) Flanking structure: dragged portion of the host fabric element (HE) close to the cross-cutting element (CE) is the "internal HE". Straight and undisturbed 'external HE'. Source: Passchier, 2001. Reproduced with permission from Elsevier.

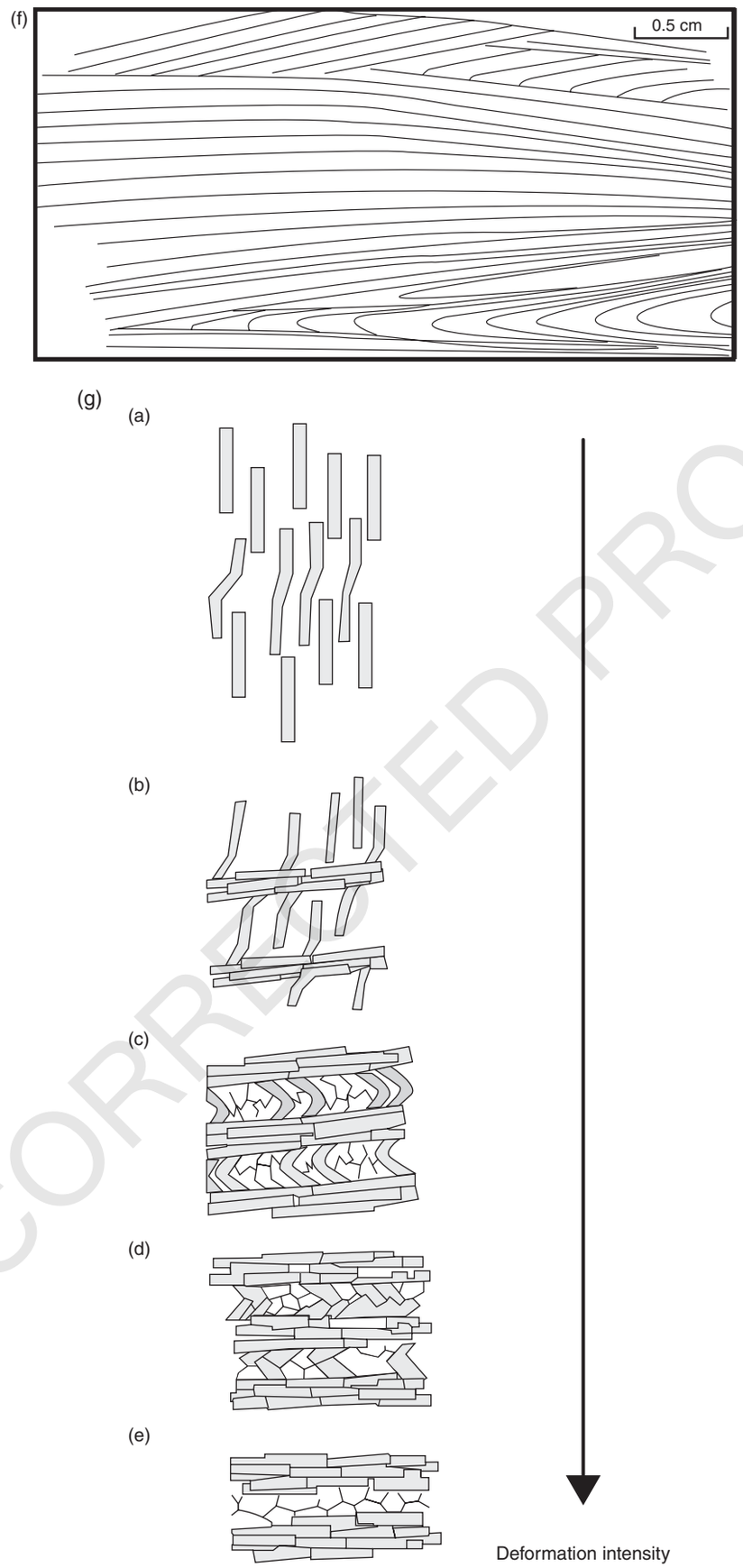

Fig. 12.3. (*Continued*) (f) A number of generations of foliations are present: some of these truncate others and one is folded. The folded foliation is bound by other foliations, hence the fold is 'intrafolial'. Source: Bell 2010. (g) How pronounced compression flattens folded lath shaped grains is shown. Source: Passchier and Trouw 2005. Reproduced with permission from Springer Science + Business Media.

and verge SW (Figs 12.4a–d, 12.5b, c, 12.6a–c). On the other hand, folds verge NE inside those two detachments (Figs 12.5a, d; 12.7a–d). Inside the ZSZ intrafolial folds also verge NE (Fig. 12.8). These folds are intrafolial *sensu stricto*, and are unrelated to different types of intrafolial folds *sensu lato* as mentioned in Section 12.3. The reasons are as follows. Many of the folded quartz aggregates documented here have significantly continuous limbs along the primary shear C-planes (Figs 12.5a–d, 12.6b, d, 12.7a, c, d, 12.9c). So unlike Fig. 12.3(a, b), they probably did not originate from initially antithetic layers. As deciphered on meso- and microscales, these folds confine within primary shear C-planes. Mukherjee (2010a) and Mukherjee and Koyi (2010a) distinguished secondary shear planes in the Sutlej section at 15–55° to the C-planes. Thus the studied folds contradict counter-rotated back-folds within secondary shear planes. The documented folds do not constitute any porphyroblast/clast system, and hence differ from mineral grains as in Fig. 12.3c. None of the studied folds are the tails of mineral grains, which are in contrast to the cases (i) and (ii) of Fig. 12.3c. The folds presented here are unassociated with any nearby structural element that cross-cut them. Therefore, these folds should not be correlated with flanking structures of Fig. 12.3e. Large-scale folds exist neither in the Sutlej section of the HHSZ (Vannay et al. 2004; Mukherjee 2007, 2010a – especially its fig. 14d; Mukherjee and Koyi 2010a) nor exclusively within the ZSZ (Patel et al. 1993; Mukherjee 2007, 2010b; Mukherjee and Koyi 2010b). Notice that the main foliations (or the primary shear C-planes) dip N/NE moderately. Therefore, these intrafolial folds do not categorize as

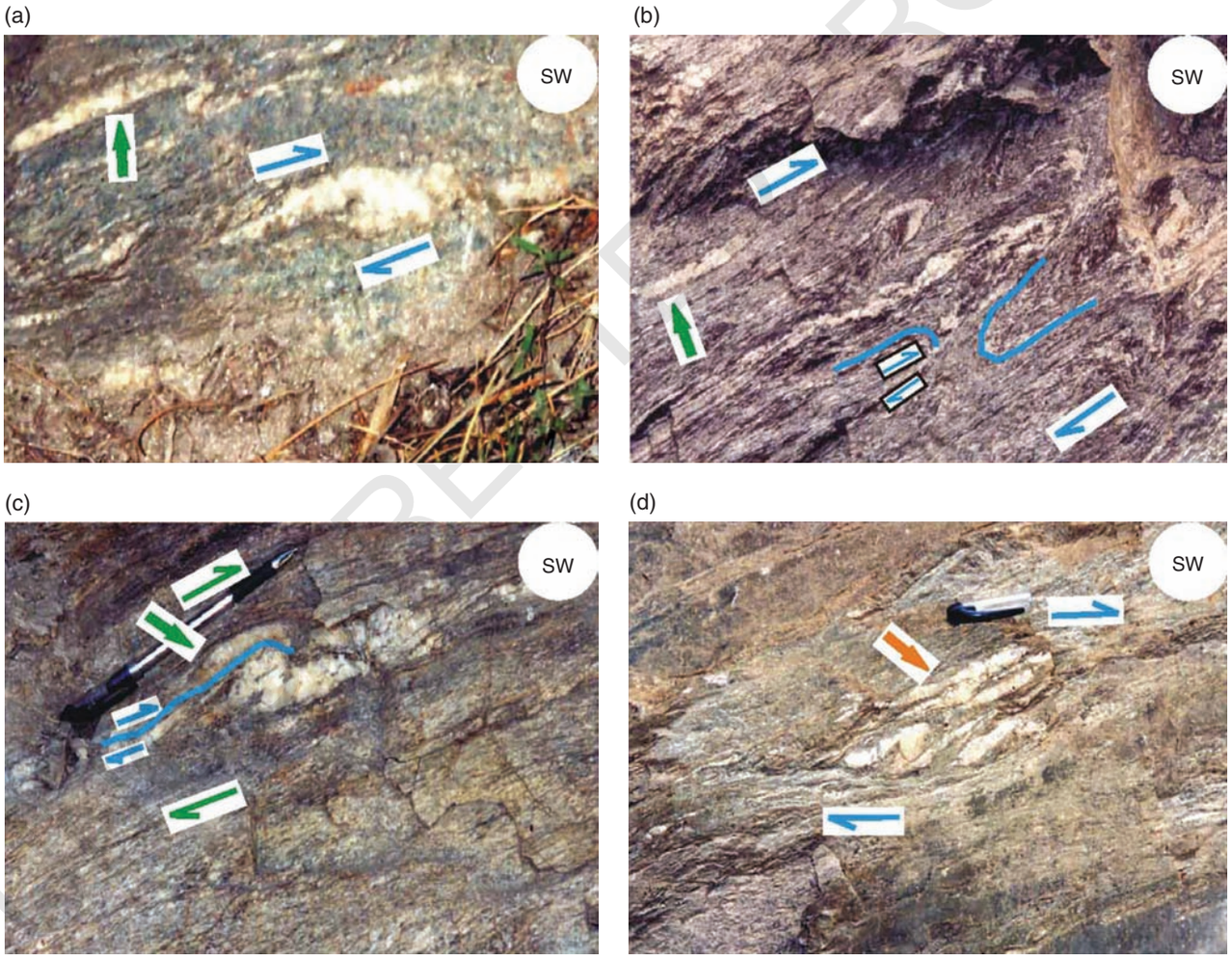

Fig. 12.4. Intrafolial folds of quartz veins that are asymmetric and overturned, from the Higher Himalayan Shear Zone, Sutlej section. Shear sense: top-to-SW (up). (a) Limbs of different thicknesses, thicker and round hinge. An intrafolial fold of different style is shown by a green arrow. Location: 6. (b) Ductile shear disrupted intrafolial folds into a number of rootless fold hinges. Brittle shear also acted along the main foliation. Thicker quartz vein along the main foliation (green arrow). Source: Mukherjee 2010a. Reproduced with permission from S. Mukherjee. Location: 15. (c) Ductile shear disrupted limb of an intrafolial fold (green arrow). The disrupted part overrode in a piggy-back manner (pair of smaller half arrows) over another fold along the main foliation. The plane of override also acted as a brittle shear plane (blue line). Location: 12. (d) Irregular adjacent folds of different morphologies, one of which is a "flame fold" with a sharp hinge (orange arrow). Source: Mukherjee 2010a. Reproduced with permission from S. Mukherjee. Location: 9.

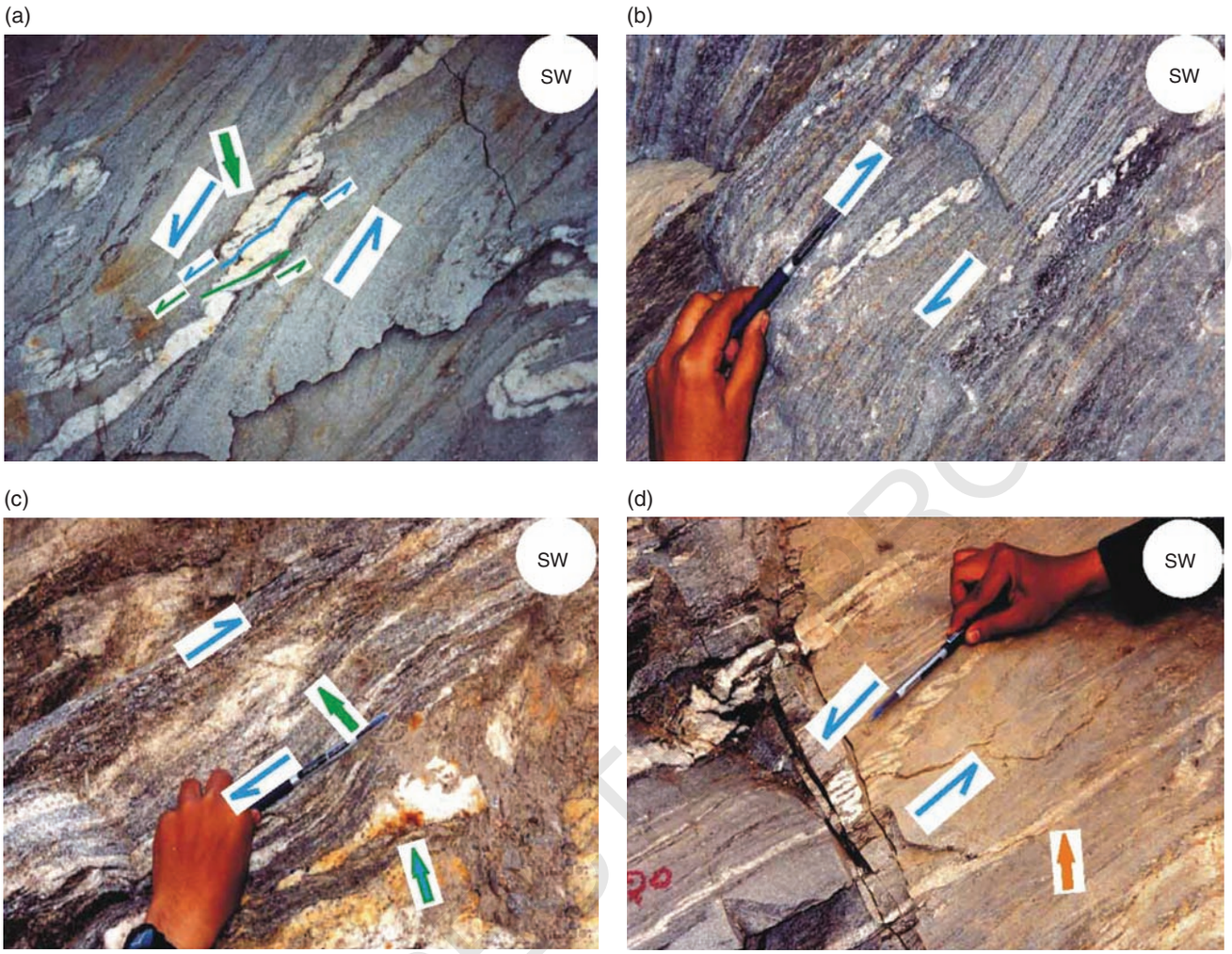

Fig. 12.5. Asymmetric overturned non-periodic intrafolial folds in a train, from the Higher Himalayan Shear Zone, Sutlej section (Fig. 12.2a). (a) Brittle shear sub-parallel to the axial trace disrupted the limbs (green and blue lines and their half arrows). The hinge zone is remarkably straight. Shear sense: top-to-NE (down). Location: 3. b. Isoclinal fold and almost a box fold in the same train. The vergence of the isoclinal fold indicates the shear sense (top-to-SW, up) but not the box fold. Source: Mukherjee 2010a. Reproduced wiuth permission from S. Mukherjee. Location: 13. This fold is plotted in Ramsay's (1967) scheme in Fig. 12.13. (c) The folded quartz vein cuts across the foliation planes (green full arrow). Shear sense: top-to-SW (up). Source: Mukherjee 2010a. Reproduced with permission from S. Mukherjee. Location: 3. (d) Thicknesses of limbs vary along the fold train. Uniform shear sense is displayed by every fold in the train. Shear sense: top-to-NE (down). Another quartz layer is nearly straight and not folded (orange arrow) Location: 2.

parasitic folds. A few hook folded leucosomes do occur within the $STDS_L$, Sutlej section (Fig. 12.7b), and on microscale within the ZSZ defined by sillimanite and quartz minerals (see Fig. 12.12a-d). They could have formed from either an undeformed marker (such as Fig. 12.3a) or a shear fabric (e.g. Fig. 12.3b) that was initially oriented antithetically. The final shear sense of top-to-NE sense as indicated by intrafolial folds *sensu stricto* matches with that interpreted from hooks (Fig. 12.7b). Three foliation sets occur repeatedly in all the study areas- two sets of the S-fabrics indicative of an earlier top-to-SW (Figs 12.4a–d, 12.5c, 12.6d) and a late phase top-to-NE ductile shear (Figs 12.5a, b, d, 12.6a–c, 12.7a–d, 12.8a–c, 12.9a–d, 12.10a–d, 12.11a–c, also Fig. 12.12). Both these sets of S-fabrics are bound by a common set of C-planes. Besides, a synthetic shear sense indicated by an S- plane and its bounding nearly straight C′-plane persist in the Sutlej section (figs. 4b, 5d, 6c, d, 8a of Mukherjee and Koyi 2010a). Thus, although multiple sets of foliations exist in the study areas, all of them have been categorized into specific deformation patterns, and they do not "randomly" cut across. It was found that the intrafolial folds are confined within the C-plane that is common to the northeast- and southwestward ductile shear. The studied intrafolial folds occur close to many other shear sense indicators such as mineral fish and sigmoid quartz veins (Mukherjee 2007, 2010a,b; Mukherjee and Koyi 2010a,b). This indicates simple shear produced those shear structures, and were not merely transposed foliations. As a NE–SW compression

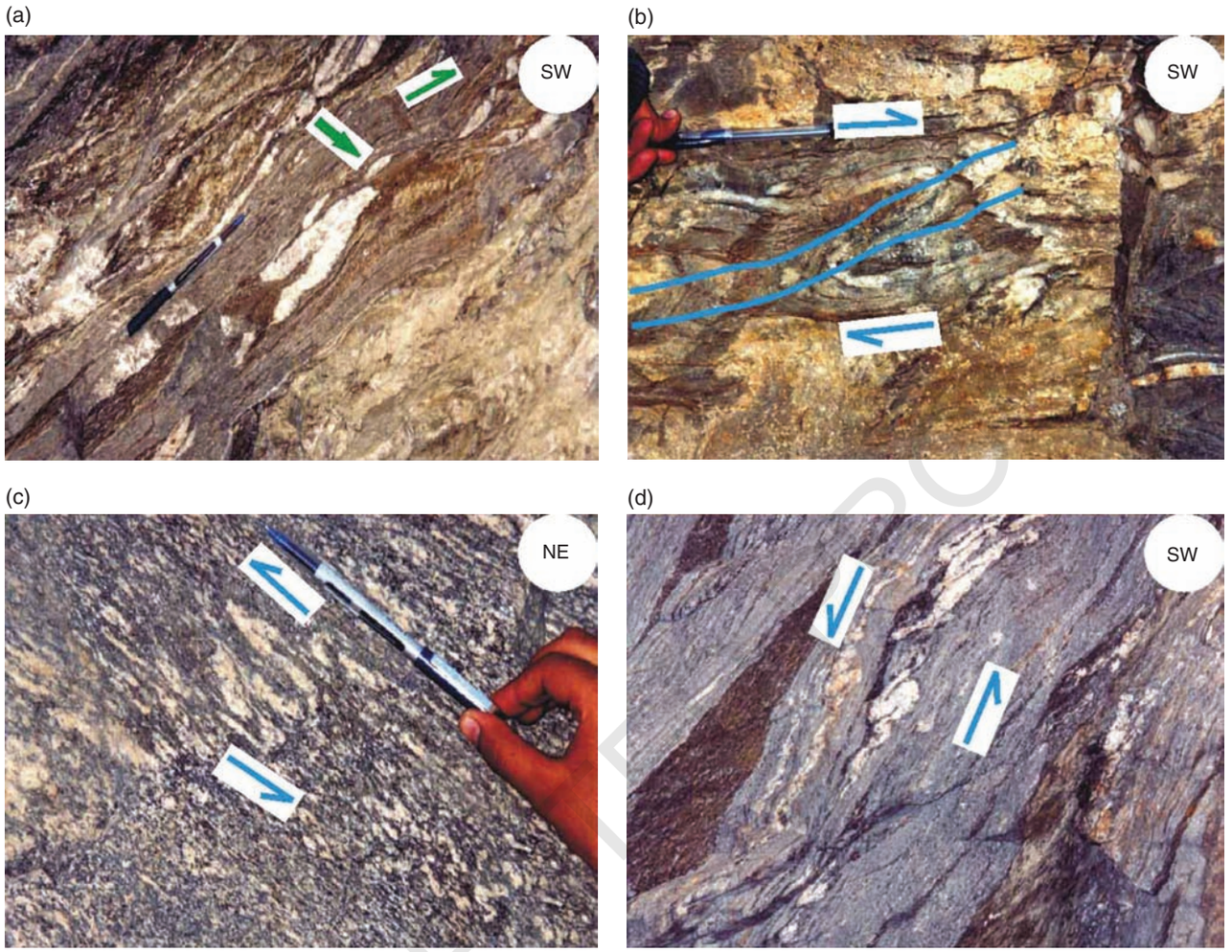

Fig. 12.6. Asymmetric overturned intrafolial folds, from the Higher Himalayan Shear Zone, Sutlej section. (a) The rootless flame fold of quartz with sharp hinge and fold axis sub-parallel to the foliation. Does not give shear sense alone. The tiny sigmoid quartz (green arrow) reveals a top-to-SW shear sense. Source: Mukherjee, 2010a. Reproduced with permission from S. Mukherjee. Location: 3. (b) Axial traces (blue lines) are somewhat curved. One of the limbs is sub-horizontal. Top-to-SW (up) shear. Location: 8. (c) S-shaped fold that truncates foliations. Top-to-SW (up) shear. Source: Mukherjee, 2010a. Reproduced with permission from S. Mukherjee. Location: 12. (d) Hinge area much thicker than the limbs. Top-to-NE (down) shear. Location: 3.

since ~55 Ma persisted in the India–Eurasia collisional regime (Keary et al. 2009), compression induced SW vergent intrafolial folding of the NE-dipping main foliation planes is one possibility, similar to Fig. 3h. However this is improbable. As argued in the previous point, it cannot explain a variety of unambiguous shear sense indicators on meso- and microscales that qualified the Higher Himalaya as a shear zone (see Jain and Anand 1988).

12.4.2 Morphology and structures

1 The two limbs of the studied individual intrafolial folds dip either SW (Figs 12.4a–d, 12.5b, c) or NE (Figs 12.5a, d, 12.6a–c, 12.7a–d, 12.8a, c, 12.9a–d, 12.10a–d, 12.11a–d). Therefore, these folds are overturned folds. Such folds are bound by primary shear C-planes (main foliations) that in the field are defined by thin planar leucosomes (Figs 12.4b, c, 12.5b–d, 12.6d, 12.7a–d), and on microscale by micas (Fig. 12.8). In the field, these fold trains can be traced for a maximum of about a meter, and in thin-section, for about a millimeter. Lengths and thicknesses of limbs of few intrafolial folds are quite dissimilar (Figs 12.4a, 12.9d, 12.10c, d, 12.11d). Most of their axial planes are straight (Figs 12.4a, d, 12.5a–d, 12.6a), but some are curved (Figs 12.6b, 12.7a, c, 12.8a–c, 12.9d; 12.10b, 12.11c). Microscopic intrafolial folds of single minerals seldom exhibit the geometries of sheared boxes and are rootless (Fig. 12.11b). A few rare observations are as follows. Shear planes can sharply truncate intrafolial folds with round hinges (Fig. 12.5a). Sometimes hinges of rootless intrafolial folds shears into flame shapes (Figs 12.5d and 12.7a; also designated as "intrafolial hinges" and "rootless lenses": Nicolas 1987).

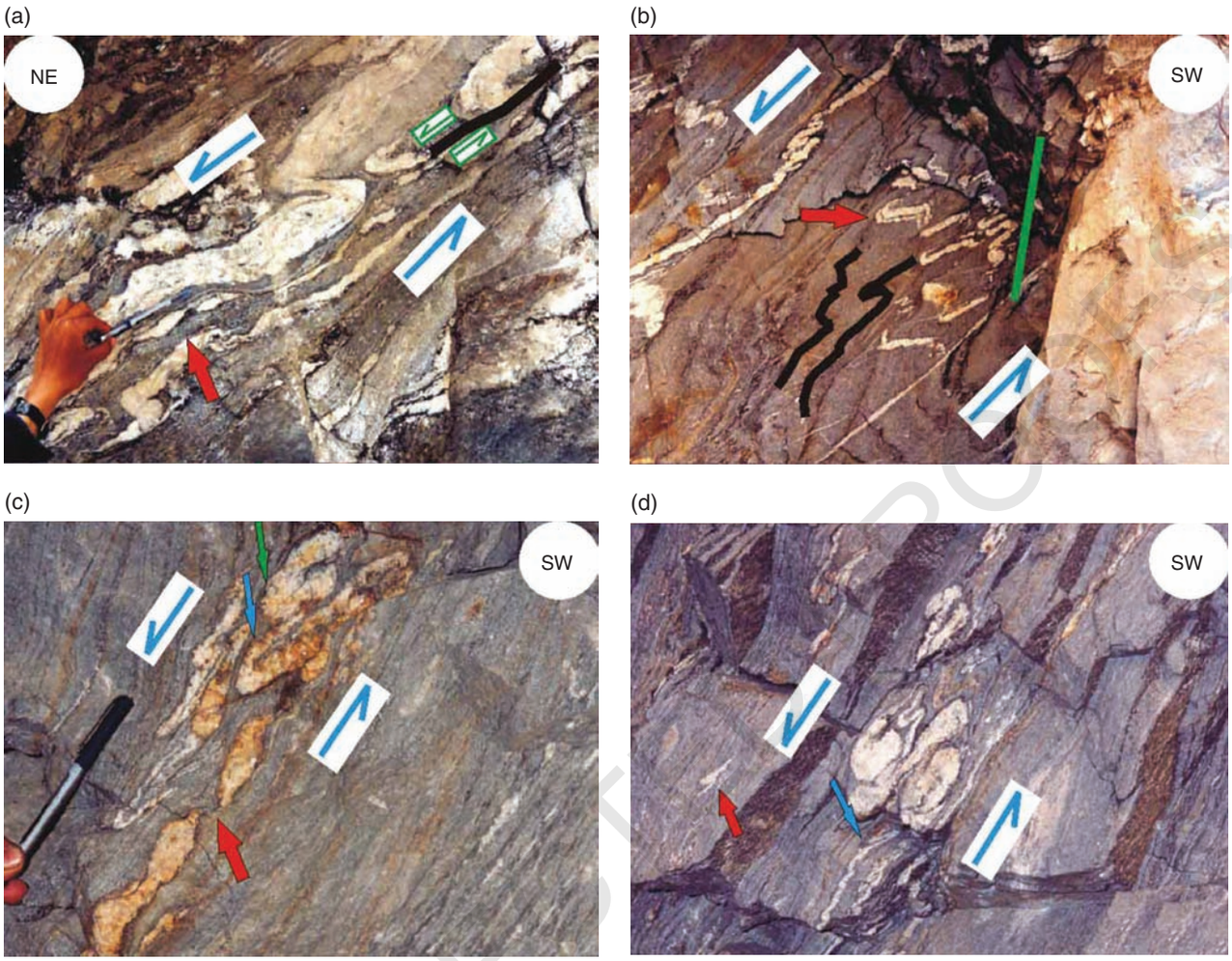

Fig. 12.7. Asymmetric overturned intrafolial folds, from the Higher Himalayan Shear Zone, Sutlej section. (a) The thicker layer of quartz shows more prominent folds. Along the main foliation, brittle faulting (green line and half arrows) disrupted the fold. Top-to-NE (down) shear sense. A top-to-SW shear is indicated by sigmoid quartz veins (orange arrow). Source: Mukherjee, 2010a. Reproduced with permission from S. Mukherjee. Location: 3. (b) Several rootless folds around the middle of the view, but only one of them have parasitic folds (orange arrow). At top-left side a continuous layer of quartz got intrafolial folded, its initial orientation with respect the shear C-plane is approximately represented by a green line. The matrix of schistose psammite is also intrafolial folded in sympathy with the quartz vein. The blue full arrow points at a fold of different style. Location: 4. (c) Folds in quartz layers with different thickness. Fold hinges of different thicknesses (blue and green full arrows). Layer parallel boudinaging took place (orange arrow) Top-to-NE (down) shear. Location: 3. (d) Side by side folds of contrasting thickness. A tiny rootless fold with well-developed hinge and limbs (orange arrow), and one more tiny intrafolial folds in a train (blue full arrow). Top-to-NE (down) shear. Location: 3.

Microscopic sheath folds and intrafolial folds (Fig. 10c) co-existing in the same field of view indicate strain partitioning over a few mm distance. This is because sheath folds are products of extreme ductile shear and can originate through intrafolial folds (Davis et al. 2012). Note that sheath folds too can be intrafolial (Andrews et al. 2005). An intrafolial fold with a hinge much thinner than its limbs (Fig. 12.10c) is unusual than the opposite case (Figs 12.4a, 12.6c, 12.6d, 12.7d, 12.10d).

2 Intrafolial folds of contrasting geometries (and sizes) sometimes occur adjacently (Figs 12.4a, 12.5c, 12.7d, 12.9c). Such changes in style and/or size can be across the trains (Figs 12.4a, 12.5c, 12.7d). Style can vary even in the same train – for example, folds with U-shaped and sheared box geometries can coexist (Fig. 12.9c).

3 Intrafolial folded quartz grains show wavy extinction under an optical microscope indicating that their optic axes rotated by folding (Fig. 12.10d). Individual recrystallized quartz grains too deform and assume shape-preferred orientation (= "oblique foliation" of Vernon 2004; Trouw et al. 2010) when the aggregate intrafolial folds. In plane polarized light, such patterns appear subtle but are decipherable (compare Fig. 12.9a and Fig. 12.9b). The oblique foliation and the fold vergence show the same ductile shear sense connoting coeval folding and the obliquity of the foliation. The following effects are deciphered when intrafolial folds undergo

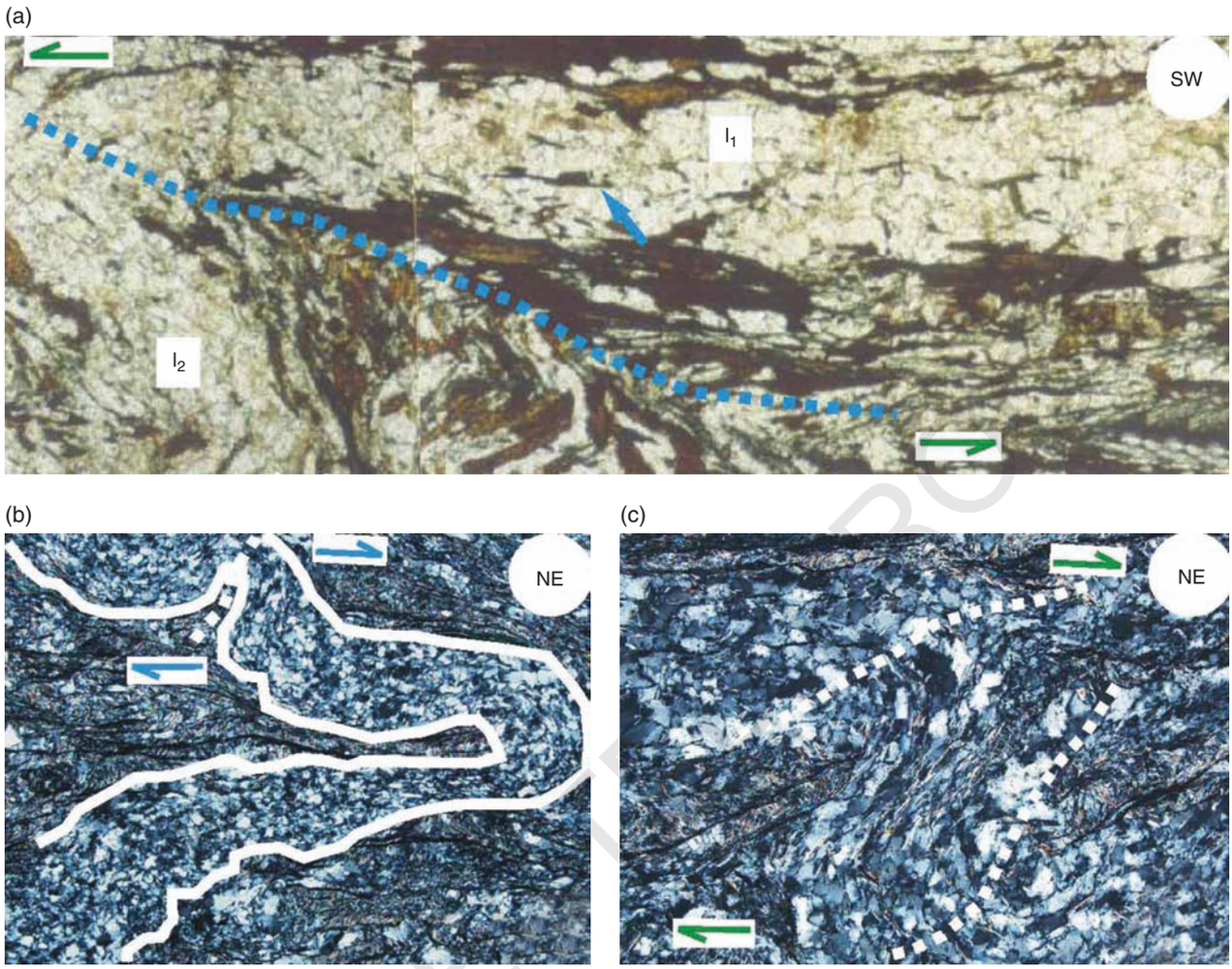

Fig. 12.8. Top-to-NE shear revealed by microscopic intrafolial folds with curved axial traces, Zanskar Shear Zone. (a) A quartz vein sub-parallel to the main foliation got round hinged folded, and maintained its longer limb (l_1) of nearly the same orientation and the shorter (l_2) at an angle. Very thin and disjointed biotites within the fold define subtle layers (blue full arrow). Thinner biotite and other quartz layers are tightly folded with sharper hinges developed in the core of the folded quartz layer. Plane polarized light. Location: P9/K. Photo length: 2 mm. Source: Mukherjee and Koyi 2010b. Reproduced with permission from Springer Science + Business Media. (b, c) The magnification of Fig. 12.8b is Fig. 12.8c: polyclinal irregular folded quartz vein. Quartz grains are elongated along folded layer. Thinner and disconnected micas also defined layers. Curved axial traces (white dash lines) define the shear sense. Location: P9/D. Photo lengths: 1 mm. Source: Mukherjee 2013. Reproduced with permission from Springer Science + Business Media.

brittle deformation. Thinning limbs thicken adjacent hinge zones so that the limbs snap. This resembles the genesis of lenticular boudins through "pinch and swell" structures (Twiss and Moores 2007). Hinge areas thicker than the limbs (especially Figs 12.4a and 12.5c) indicate that materials flowed from the limbs towards the hinges during folding. The disrupted portion of an intrafolial fold can thrust over the hinge of an adjacent fold along a local brittle plane. This brittle plane in such a case parallels the ductile shear plane that bounds the fold (Fig. 12.4c). Brittle shear of limbs of intrafolial folds occur at an obtuse angle to the shear direction and sub-parallel the axial traces (Fig. 12.5a). These shears confine solely within the folded layer and not within the matrix. This indicates that the local brittle shears acted during the progressive evolution of the intrafolial folds, and did not relate to regional tectonics. Likewise, fractures nearly orthogonal to the limbs confine entirely to the limbs. These fractures are not perfectly straight (Figs 12.9a and 12.10a), and are unrelated to the mesoscopic deformation structures/fabrics. Some of the fractures developed only at one of the margins of the folds (Fig. 12.9a). In a very rare case, a Y-shaped fracture formed inside the fold but did not reach any margin (Fig. 12.9a). A fracture can subparallel axial trace (Fig. 12.11d).

4 On mesoscopic scales, intrafolial folds of quartz aggregates are devoid of internal mica layers (Fig. 12.4a–d). On the other hand, on microscales, the folded quartz aggregates develop foliations defined by micas in one

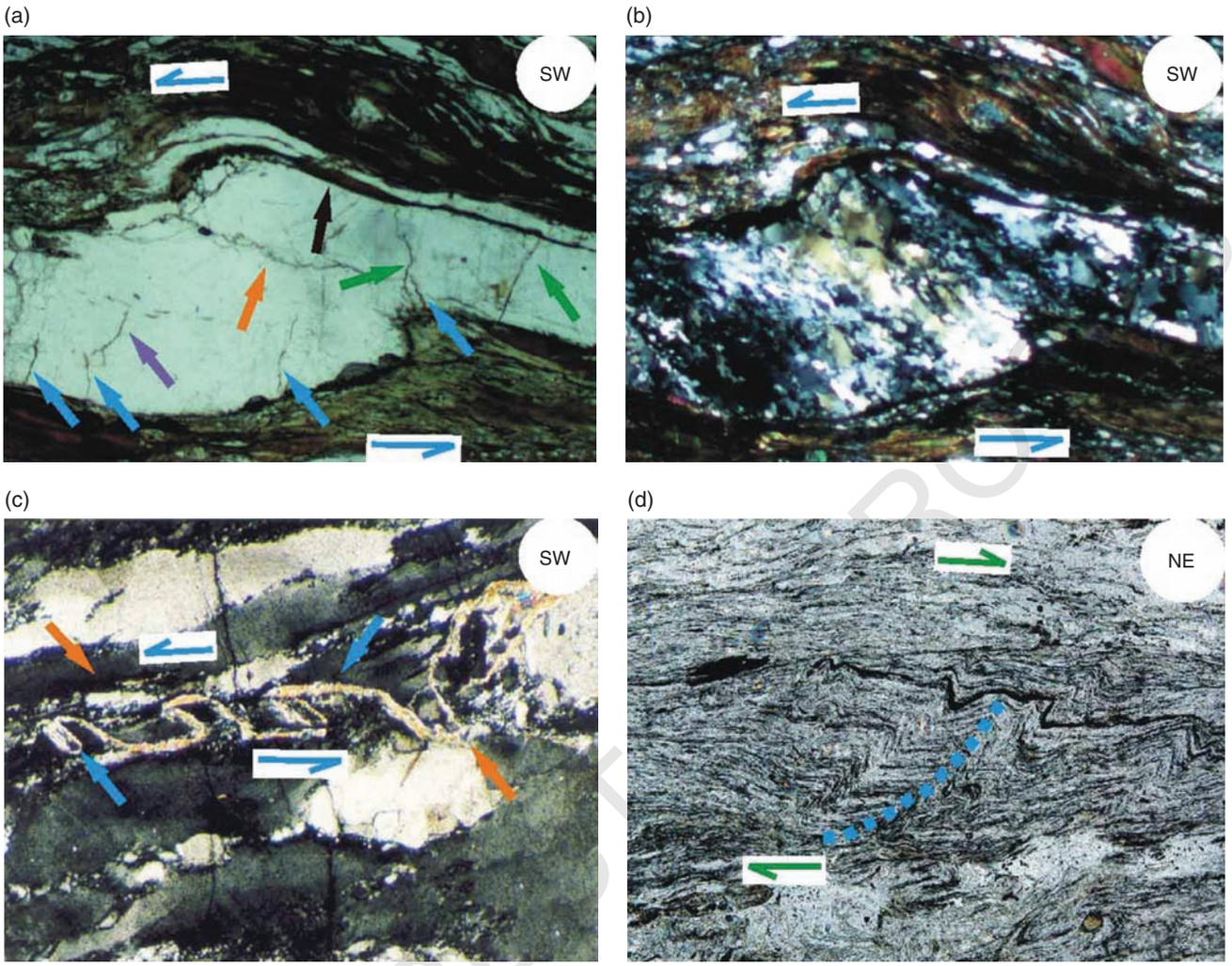

Fig. 12.9. (a.b) Intrafolial folds under microscope from the Zanskar Shear Zone. Few fractures only at the margins (blue full arrows), a few of which cross the complete limb (green full arrows). A Y-shaped fracture network formed inside the fold (purple full arrow). A much thinner layer of biotite occurs only at one of the margins of the folded quartz grain (black full arrow). Location: P9/K. Photo length: 3 mm. (a) Plane polarized light. (b) Cross-polarized light. Source: Mukherjee and Koyi 2010b. Reproduced with permission from Springer Science + Business Media. (c) Mylonitic foliation defined by train of micas is intrafolial folded into asymmetric overturned U- and box shaped folds (blue full arrows). Shear planes are defined by elongated recrystallized quartz grain and straight grain boundary (orange arrows). Cross-polarized light. Photo length: 2 mm; Location: P9/G. Source: Mukherjee 2013. Reproduced with permission from Springer Science + Business Media. (d) Kinked mica layers with SW dipping axial traces. Plane polarized light. Photo length: 1 mm. Source: Mukherjee 2013. Reproduced with permission from Springer Science + Business Media.

of the following ways: (i) as separated grains but of same orientation (Fig. 12.8a); (ii) as grains in close continuation and in several layers (Fig. 12.8b, c); and (iii) an aggregate of grains occurring at a part of the fold (Fig. 12.9a). In these cases, foliation planes inside the folds mimic the later (like "F" in Fig. 12.2f). This indicates that the studied intrafolial folds with the same shear sense are not recycled, unlike Fig. 12.2a.

5 Our study of 42 intrafolial folds, both isolated/rootless and in trains in the Sutlej section, and another 18 in thin-section from the ZSZ reveal that the vast majority (e.g. Figs 12.13 and 12.14) plot within the Class 1C of Ramsay's (1967) scheme of fold classification. Ramsay (1967) defined t′ as the orthogonal thickness at a point on the fold limb divided by that at its hinge. Similarly, T′ is the ratio of the axial planar thicknesses. α is the acute angle between the tangent drawn at the point on the fold limb where the dip isogon was drawn. The plots sub-parallel the Class 2 line in the graphs of t′ vs α (Figs 12.13a, 12.14a), and Class 1B lines on T′ vs α (Figs 12.13b, 12.14b). These plots, however, cannot compare with figs. 7–79 and 7.80 of Ramsay (1967). These two figures consist of plots that parallel Class 2 and the Class 1B lines and were used to estimate fold related flattening (also see caption of fig. 1c of Hudleston and Lan 1993). This is because Ramsay's

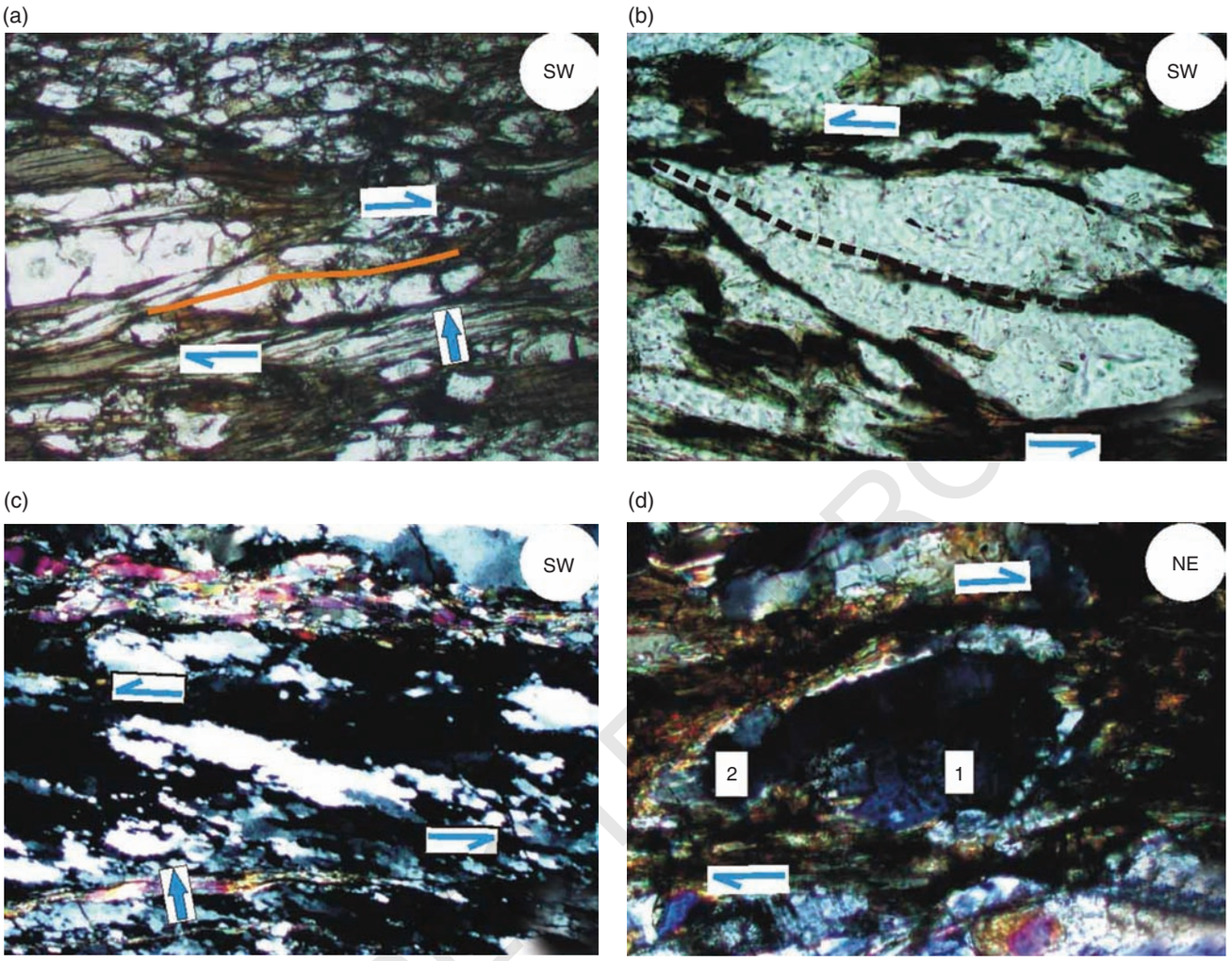

Fig. 12.10. Intrafolial folds of quartz under microscope, Zanskar Shear Zone. Shear sense: top-to-NE. (a) Axial trace at low angle to the C-foliation (green line). Boudinaged limbs (blue full arrow). Plane polarized light. Photo length: 2 mm; Location: P9/A. (b) Rootless fold. A few biotite grains inside it define a curved axial trace (blue dash line). Plane polarized light. Location: P9/O. (c) Remarkable difference in length of limbs of the folded recrystallized quartz grains. A sheath fold of quartz also present (blue full arrow). Cross-polarized light. Location: P9/G. Photo length: 3 mm. (d) Rootless fold with irregular boundaries. Wavy extinction of folded quartz grain. Limbs 1 and 2 are marked and are plotted in Ramsay's (1967) scheme in Fig. 12.14. Cross-polarized light. Photo length: 1 mm. Location: P9/B.

(1967) exercises apply only to parallel geometries of the initial folds. Whether the studied intrafolial folds were at their initial stages of parallel geometries, however, is indeterminate.

Hook folds fall in Class 3 in t′ vs α and T′ vs α graphs (Fig. 12.15a,b). This means that retro shear on a pre-existing intrafolial fold can significantly alter its geometry into a stronger curvature of the outer arc than the inner one (of every Class 3 folds). Irregular margins of some microscopic intrafolial folds (Figs 12.4a, 12.9a, 12.10c, d) and hooks (Fig. 12.12a, c) probably arose due to migration of adjacent grains (Passchier and Trouw 2005) towards the former. We manually smoothed grain-scale irregularities on tracings sheets before measuring for Ramsay's (1967) graphs. Had we not done this, the irregularities would have rendered the plots haphazard. Such smoothening has been a standard process of fold analyses (e.g. Singh 2010). Many of the mesoscopic folds had rather even margins (Figs 12.6d and 12.7a). We did not require best-fit curves for them.

The plots for intrafolial folds (Figs 12.13, 12.14) and hooks (Fig. 12.15) show the final geometries and cannot decipher fold evolution as shearing progressed. However, analyses of the few figs. published on the progressive development of intrafolial folds from irregular layers by Bons and Jessel (1998) reveal that at an overturned fold (limbs "c" and "d" in Fig. 12.2f) plots within Classes 1C and 2. On the other hand, folds in the same train with limbs initially dipping in opposite directions (limbs "e" and "f" in Fig. 12.2f) more closely follow a Class 2 pattern (Fig. 12.16). Initially a Class 1C fold of Fossen (2010;

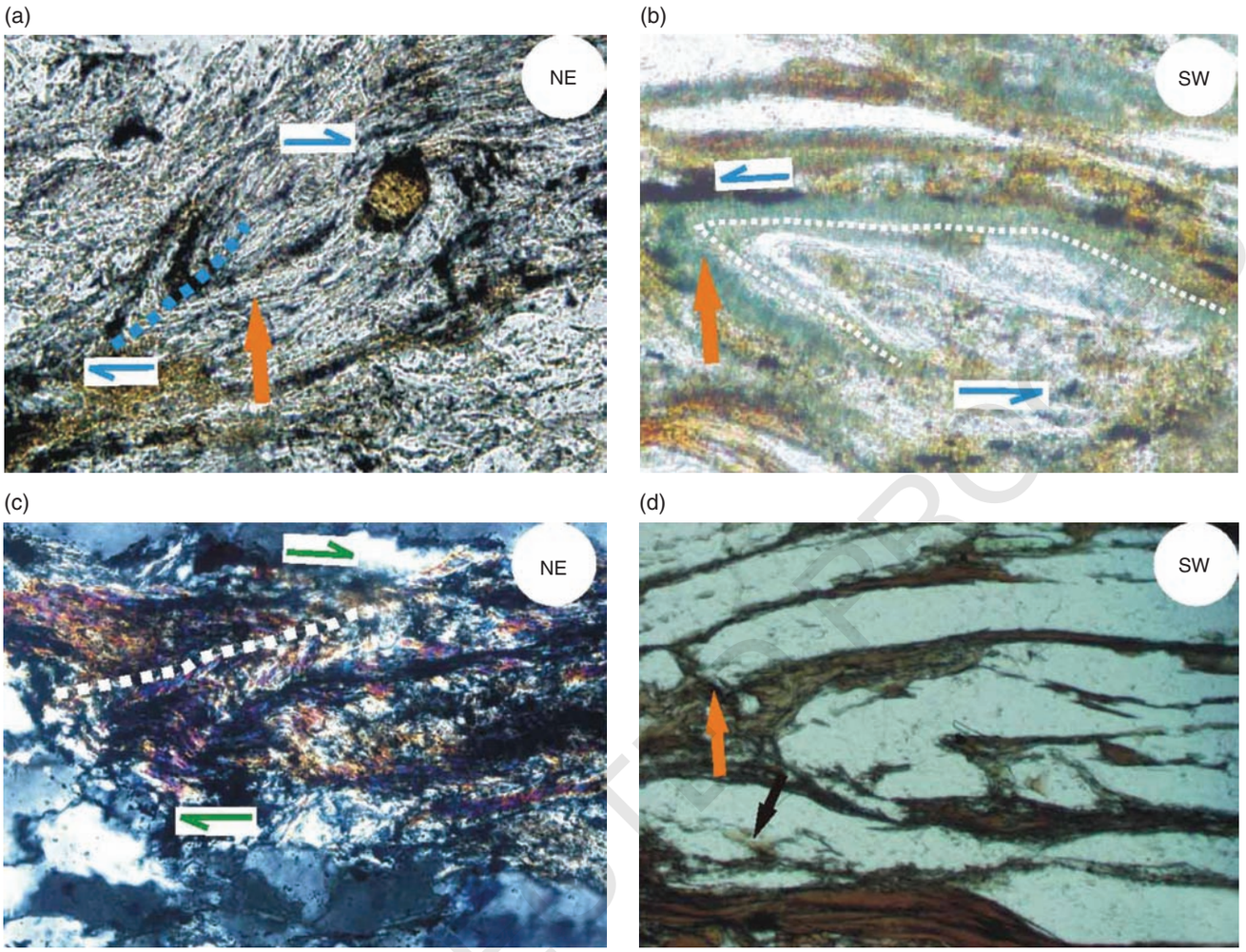

Fig. 12.11. Microscopic intrafolial folds from the Zanskar Shear Zone, shear sense: top-to-NE. (a, b) Rootless folds of sillimanite (orange arrows). That on the left has a sharp hinge whereas that on the right is more like a 'sheared box fold'. Photos in plane polarized light. Photo lengths: 1 mm; Location: P9/N. Source: Mukherjee and Koyi 2010b. Reproduced with permission from Springer Science + Business Media. (c) Crenulated mica aggregate reveal the shear sense. Axial trace (white dash line) is curved. Photo in cross-polarized light. Photo lengths: 1 mm; Location: P9/D. Source: Mukherjee, 2013. Reproduced with permission from Springer Science + Business Media. (d) Fracture developed along the axial trace in a few folds (black full arrow). One of the limbs is tiny (orange arrow). Photo in plane polarized light. Photo lengths: 2 mm; Location: P9/C.

here Fig. 12.2c) maintained a Class 2 geometry as simple shear progressed (Fig. 12.17). Apart from the hooks, we avoided analysis of the intrafolial folds *sensu lato* mentioned in Section 12.3.2.

12.4.3 Shear sense

Intrafolial folds with opposite vergence in the same rocks or shear zones were not encountered. Furthermore, the vergence of intrafolial folds always matched with nearby shear sense indicators such as S-C fabrics, mineral fish and asymmetric quartz veins (Figs 12.5c, 12.7a, but many others outside the field of view of the photos). We therefore consider the studied intrafolial folds to be reliable ductile shear indicators. In a single train, shear sense can be deduced unambiguously from folds that are overturned or are asymmetric with axial traces at moderate angles to the shear planes (especially Figs 12.4a, d, 12.5a, 12.7a, c, 12.8a, b, 12.9a–d, 12.10a–d, 12.11a–c). In a polyclinal fold, some of the axial traces subparallel the main foliation – and so cannot indicate the sense (Fig. 12.8b). Instead, only those subfolds with the inclined axial traces within the fold give unequivocal shear sense (Fig. 12.8b). Interestingly, from the present orientation of hook-shaped intrafolial folds (*sensu lato*, as in Fig. 12.12a, c) of single minerals, in microscopic examples from the ZSZ, the relative time relation of ductile shear – first a top-to-SW and then a top-to-NE – could be interpreted. However, noting that hooks can also form from initially antithetically oriented markers (as in Fig. 12.3b), the interpretation cannot be confirmed. Further, the curved axial traces of intrafolial folds resemble S-fabrics

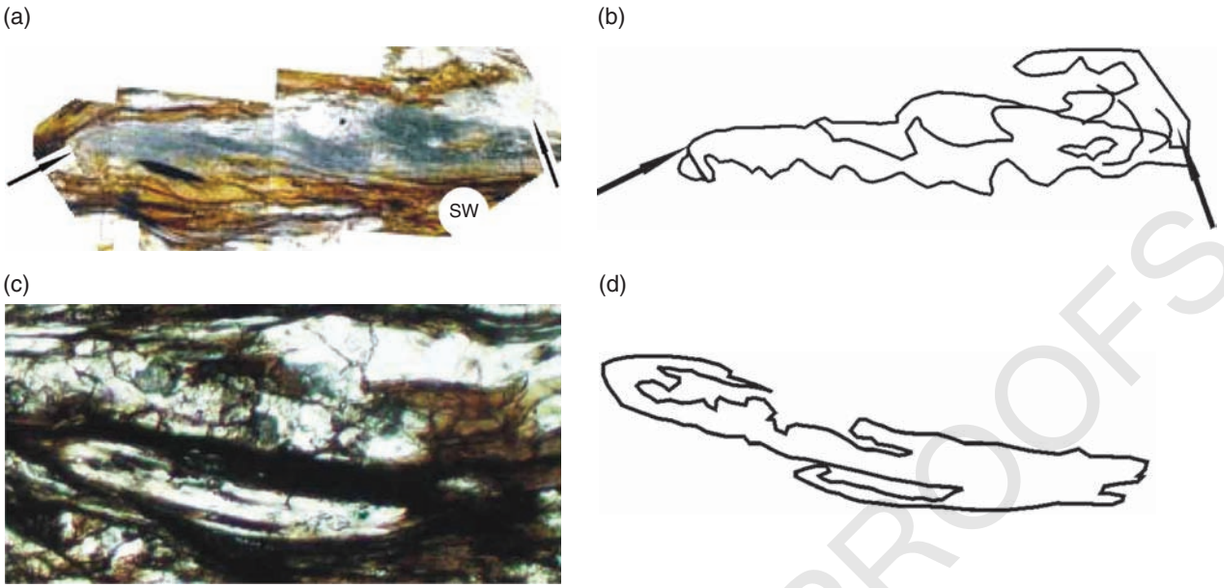

Fig. 12.12. (a) A rootless intrafolial folded sillimanite, from Zanskar Shear Zone. Note curvature of the grain at the two ends (arrows). Plane polarized light. Photo length: 1 mm; Location: P9/N. (b) Sillimanite of Fig. 12.11 is outlined. (c) A quartz hook. Cross-polarized light. (d) Outline of quartz hook. Photo length: 1 mm. Location: P9/B. It has been plotted in Ramsay's (1967) scheme in Fig. 12.15. (a, c) Source: Mukherjee and Koyi 2010b. Reproduced with permission from Springer Science + Business Media.

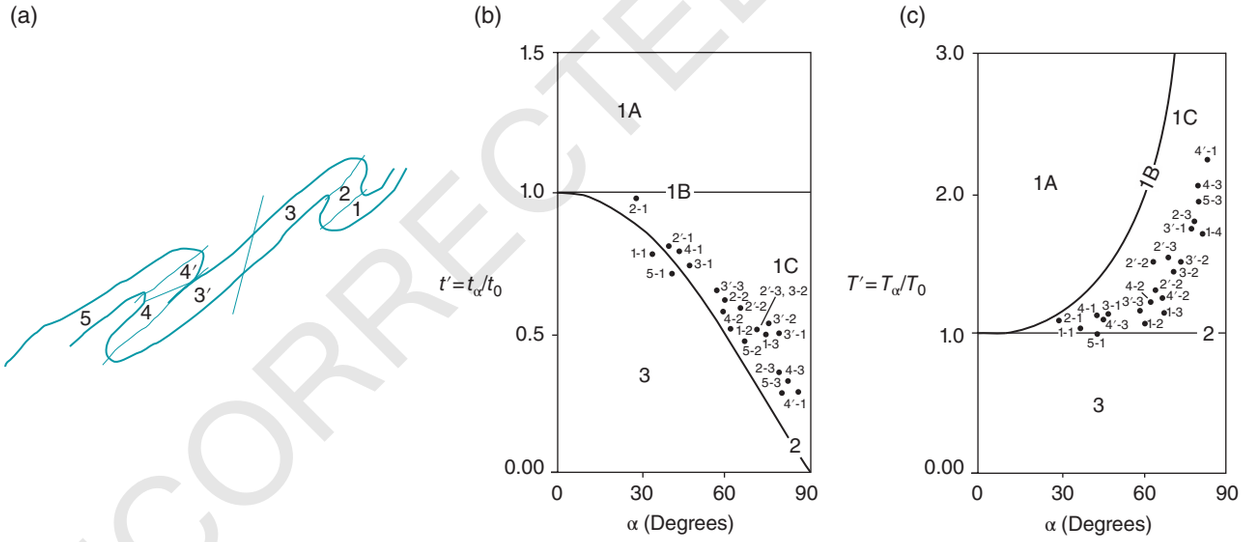

Fig. 12.13. Plot of intrafolial folds of the Higher Himalayan Shear Zone, Sutlej section in a single train into Ramsay's (1967) classification scheme. (a) The fold that was plotted is redrawn from fig. 113.2 of Bons and Jessel (1998). Limbs c, d, f, and g are marked and are plotted in Ramsay's (1967) scheme. (b) Plot of t' vs. α. (c) Plot of T' vs. α. Numbers such as 2′-1 indicate data for limb-2′ and data number 1.

(Fig. 12.6b,–c, 12.7a, c, 12.8a–c, 12.9d, 12.10b, 12.11c) and can also give the true shear sense.

12.5 DISCUSSION AND CONCLUSIONS

Locally overturned folds in ductile shear zones formed during shear and confined within primary shear planes are commonly referred as intrafolial folds. These folds usually have round hinges and thinner limbs of unequal lengths. They can either cut the adjacent foliations or parallel them. Intrafolial folding by ductile shear either reorient pre-existing planar foliations, or fold foliations around rigid inclusions. Pronounced shear leads materials in the folded layer to flow from limbs to the hinges until the limbs rupture into rootless folds. Axial planes progressively rotate to gentler inclinations to the enveloping foliation. In the plane perpendicular to the main

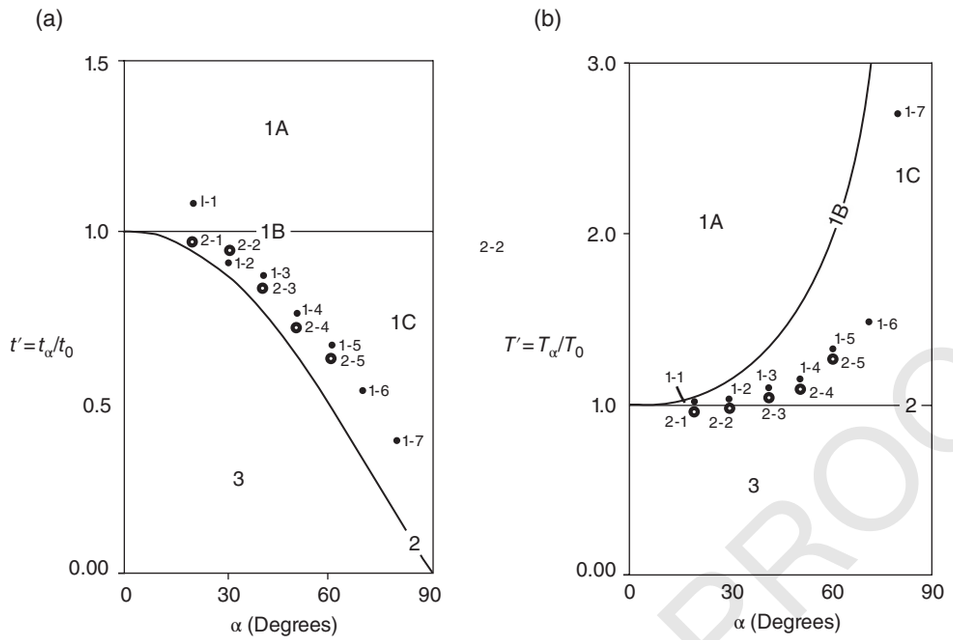

Fig. 12.14. Plot of the microscopic fold in Fig. 12.10d from the Zanskar Shear Zone into Ramsay's (1967) classification scheme. (a) Plot of t' vs. α. (b). Plot of T' vs. α. Symbols such as 1–1 indicate data from limb '1' and data number 1.

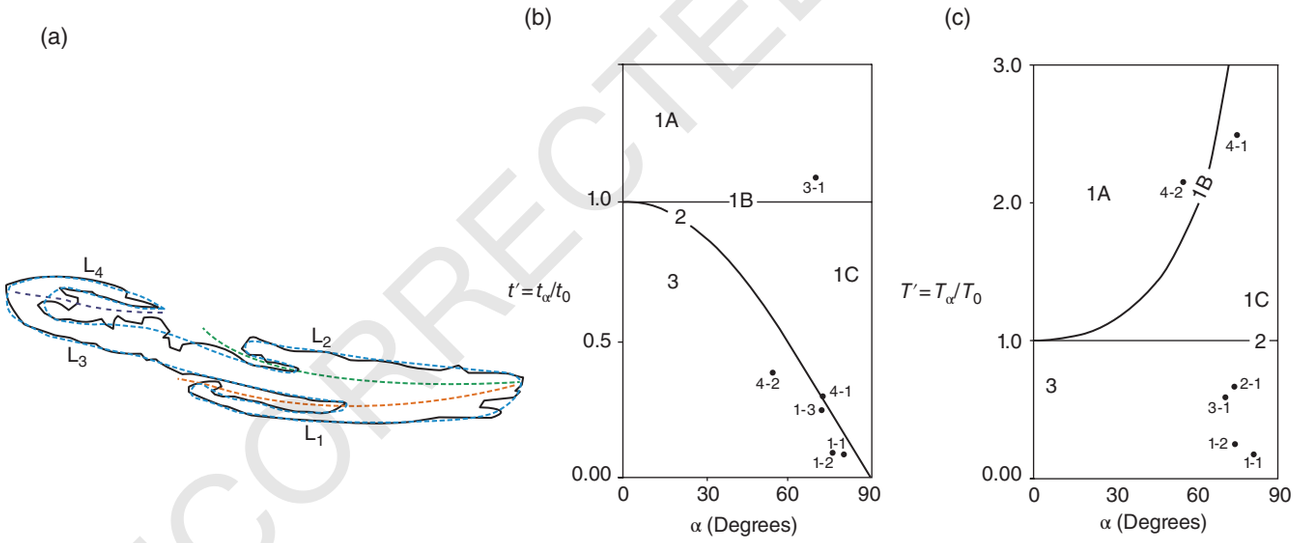

Fig. 12.15. Plot of hook shaped folds into Ramsay's (1967) classification scheme. Dashes indicate smoothening made before measurements. (a) The fold that was plotted (outlined from Fig. 12.12c). (b) Plot of t' vs. α. (c) Plot of T' vs. α. Numbers such as '4–4' indicate data for limb-4 (L_4) and data number 1.

foliation and parallel to the stretching lineation (the XZ section), intrafolial folds show the same shear sense as other shear indicators. This holds if these folds are unrelated to any major folds.

The other varieties of intrafolial folds *sensu lato* are: (i) those produced by shear of (un)deformed foliations antithetic to the shear planes; (ii) co- and counter rotated fabrics inside sheared lenses affected by secondary shear; (iii) folding of tails of some porphyroblasts; (iv) folded minerals; (v) drag folds of host fabric elements near cross-cutting elements; (vi) parasitic folds of first generation flexure slip folds; (vii) folded foliation cut by a straight foliation; (viii) folds transposed by layer parallel compression of a pre-existing fold; and (ix) folds produced by compression stronger than a perpendicular shear.

We argue that intrafolial folds within NE dipping primary shear C-planes of the $STDS_U$ and the $STDS_L$, and outside them, of the Sutlej section of the HHSZ (Himachal

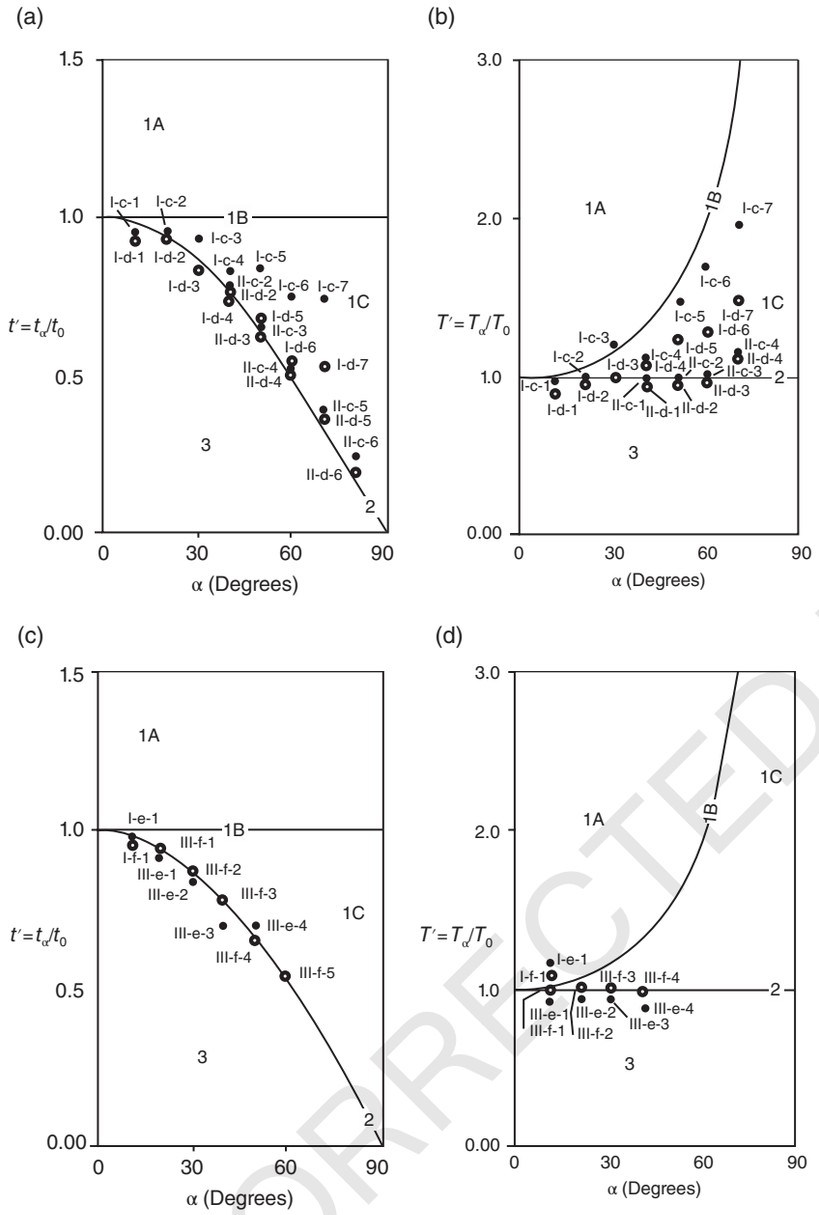

Fig. 12.16. Plot of the fold of Fossen (2010; reproduced here in Fig. 12.2(c) into Ramsay's (1967) classification scheme. Symbols such as I-a-1 indicate data from fold I, of limb 'a' and data number 1. (a, c) Plot of t' vs. α. (b, d) Plot of T′ vs. α. For each graph, two diagrams are used to avoid superposition of large number of plots. Plot of IV-a-1 to IV-a-IV, and IV-b-1 to IV-b-4 coincides with III-a-1 to III-a-IV, and IV-b-1 to IV-b-4, respectively, and are not shown in the graph to avoid crowding.

Pradesh) and in the ZSZ – an extension of the $STDS_U$ in Kashmir, do not belong to any of the categories of folds mentioned in the previous paragraph. Of regional significance are that- these folds indicate a consistent top-to-NE ductile shear, and are neither parasitic to any large scale folds, nor were they produced by the NE-SW compression related to India–Eurasia collision.

Round hinges and usually unequal limbs characterize our intrafolial folds. Some hinges are flame-shaped. Ductile or brittle shear planes can cut round hinges along axial surfaces. Both rootless folds and sheath folds indicate intense shear. Differently shaped intrafolial folds, along and across the same train, indicate deformation partitioning. Obliquity of foliation during shear, and wavy extinction of individual mineral grains characterize microscopic intrafolial folds. Pronounced shear of these folds snap the thinning limbs. Secondary shears inside the folded layers have no regional implication.

Intrafolial folds do not indicate a consistent shear sense when, either their axial traces sub-parallel the C-planes, or are polyclinal. Our observed hook-shaped intrafolial folds of a quartz- and a sillimanite grain from the ZSZ may indicate a top-to-SW followed by a top-to-NE ductile shear.

In a series of centrifuge analogue models, Godin et al. (2011), Yakymchuk et al. (2012), Harris et al. (2012a,b) studied how channel flow extrusion modifies fold geometry by dragging adjacent layers. However, these drag folds formed outside the channel flow regime and so cannot correlate with the intrafolial folds present inside

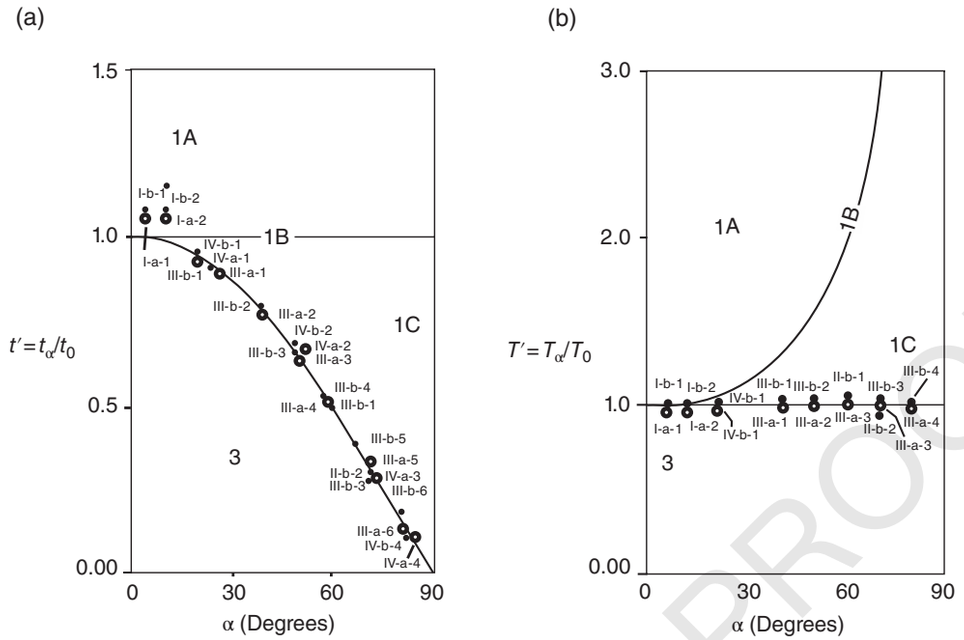

Fig. 12.17. Plot of few of the folds of Bons and Jessel (1998) into Ramsay's (1967) classification scheme. Symbols such as I-c-1 indicate data from fold I, of limb 'c' and data number 1. (a) Plot of t′ vs. α. (b) Plot of T′ vs. α. Plot II-c-1 and II-c-2 coincide with I-c-2 and I-d-2, respectively, III-g-1 and III-h-1 coincide with I-g-1 and I-h-1; therefore the former set of points are not shown.

the detachments (the $STDS_U$ and the $STDS_L$ in the Sutlej section, and the ZSZ). This is because folds in this study formed inside the putative channel of the HHSZ. Second, based on U-Pb geochronology of zircons and structural geology, Larson et al. (2010) proposed that by ~35.4 Ma, crustal thickening developed upright folds near the upper part of the HHSZ in the Nepal Himalaya. From ~22.8 Ma onwards, a top-to-SW ductile shear associated with crustal-scale channel flow rotated those folds to verge SW. Thus, Larson et al.'s (2010) model cannot explain most of the NE vergeing intrafolial folds in the study areas.

Shear fabrics of leucosomes in migmatites developed during shear (Marchildon and Brown 2003; Hasalova´ et al. 2011), which is here of a top-to-NE sense inside the Higher Himalayan detachments. Following this, intrafolial folded leucosomes in the $STDS_U$ and the $STDS_L$ of the Sutlej section (Figs 12.5a–d, 12.6d, 12.7a–d) might emplaced during ductile shearing at ~15–54 and ~14–42 Ma, respectively. This matches with Mukherjee and Koyi (2010a), who suggested extensional ductile shear (normal shear sense) in detachments acted during those time periods.

Pure sheared Newtonian viscous layer within a non-Newtonian matrix develop folds with limbs dipping in opposite directions (Ord and Hobbs 2013). Thus, those folds are not overturned. On the other hand, simple shear applied at an angle to a series of non-Newtonian layers too develop symmetric folds (Schmalholz and Schmid 2012). In none of these cases of deformation other than ductile shear, the typical overturned geometry of intrafolial folds develops.

ACKNOWLEDGMENTS

Supported by Department of Science and Technology's (New Delhi) grant: IR/S4/ESF-16/2009(G). J.N.P. and R.M. worked as Teaching Assistants. Figs 12.8b,c and 12.11c come from Roberto Weinbergs' (Monash University) thin-section. Internal and external review by several persons is acknowledged.

REFERENCES

Allaby M. 2013. A Dictionary of Geology & Earth Sciences, 4th edition. Oxford University Press, Oxford.

Aller J, Bobillo-Ares NC, Bastida F, Lisle RJ, Menéndez CO. 2010. Kinematic analysis of asymmetric folds in competent layers using mathematical modeling. Journal of Structural Geology 32, 1170–0184.

Alsop GI, Holdsworth RE. 2004. Shear zone folds: records of flow perturbation or structural inheritance? In Flow Processes in Faults and Shear Zones, edited by G.I. Alsop, R.E. Holdsworth, K.J.W. McCaffey, and M. Hand, Geological Society of London, Special Publication, vol. 224, pp. 177–799.

Andrews GDM. Branney MJ. 2005. Folds, fabrics and kinematic criteria in rheomorphic ignimbrites of the Snake River Plain, Idaho: Insights into emplacements and flow. In Interior United Western States: Geological Society of America Field Guide, edited by J. Pederson and C.M. Dehler, Geological Society of America, vol. 6, pp. 311–127.

Beaumont C, Jamieson RA. 2010. Himalayan-Tibetan orogeny: channel flow versus (critical) wedge models, a false dichotomy. In Proceedings for the 25th Himalaya-Karakoram-Tibet Workshop: US Geological Survey, edited by M.L. Leech et al., Open-File Report 2010–0099, 2 p. [Online] http://pubs.usgs.gov/of/2010/1099/beaumont/ (accessed 27 May 2015).

Becker A. 1995. Conical drag folds as kinematic indicators for strike-slip fault motion. Journal of Structural Geology 17, 1497–7506.

Bell TH. 2010. Deformation partitioning, foliation successions and their significance for orogenesis: hiding lengthy deformation histories in mylonites. In Continental Tectonics and Mountain Building: The Legacy of Peach and Horne, edited by R.D. Law, R.W.H. Butler, R.E. Holdsworth, M. Krabbendam, and R.A. Strachan, Geological Society of London, Special Publication, vol. 335, pp. 275–592.

Best M. 2006. Igneous and Metamorphic Petrology, 2nd edition. Blackwell, Oxford, pp. 423, 552.

Billings MP. 2008. Structural Geology, 3rd edition. Prentice-Hall of India Pvt Ltd., Delhi, pp. 54–45.

Bobyarchick AR. 1998. Foliation heterogeneities in mylonites. In Fault Related Rocks, edited by A. Snoke, J. Tullis, and V.R. Todd, Princeton University Press, Princeton, pp. 302–203.

Bons PD, Jessel MW. 1998. Folding in experimental mylonites. In Fault-Related Rocks, A Photographic Atlas, edited by A. Snoke, J. Tullis, and V.R. Todd, Princeton University Press, Princeton, pp. 366–667.

Burchfiel BC, Chen Z, Hodges KV, et al. 1992. The South Tibetan Detachment System, Himalayan orogen: extension contemporaneous with and parallel to shortening in a collisional mountain belt. Geological Society of America Special Paper 269, 1–41.

Carreras J, Druguet E, Griera A. 2005. Shear zone-related folds. Journal of Structural Geology 27, 1229–9251.

Chambers J, Parrish R, Argles T, Harris N, Mattew H. 2011. A short duration pulse of ductile normal shear on the outer South Tibetan detachment in Bhutan: alternating channel flow and critical taper mechanics of the eastern Himalaya. Tectonics 30, TC2005.

Davis GH, Cox LJ, Ornelas R. 1998. Protomylonite, augen mylonite and protocataclasite in granitic footwall of a detachment fault. In Fault-Related Rocks, A Photographic Atlas, edited by A. Snoke, J. Tullis, and V.R. Todd, Princeton University Press, Princeton, pp. 160–061.

Davis GH, Reynolds SJ, Kluth CF. 2012. Structural Geology of Rocks and Regions, 3rd edn. John Wiley & Sons, Inc., New York.

Dennis JG. 1987. Structural Geology: An Introduction. Wm. C. Brown Publishers, Dubuque, pp. 182, 196.

Dèzes PJ, Vannay JC, Steck A, Bussy F, Cosca M. 1999. Synorogenic extension: Quantitative constraints on the age and displacement of the Zanskar shear zone. Geological Society of America Bulletin 111, 364–474.

Duebendorfer EM, Sewall AJ, Smith EI. 1990. An evolving shear zone in the Lake Mead area, Nevada. In The Saddle Island Detachment, edited by B.P. Wernicke, Geological Society of America Memoir 176, 77–77.

Ez V. 2000. When shearing is a cause of folding. Earth Science Reviews 51, 155–572.

Fossen H. 2010. Structural Geology. Cambridge University Press, Cambridge, UK, pp. 230, 255, 303, 304.

Gangopadhyay PK. 1995. Intrafolial folds and associated structures in a progressive strain environment of Darjeeling-Sikkim Himalaya. Proceedings of the Indian Academy of Science 104, 523–337.

Gawthrope RL, Clemmey H. 1985. Geometry of submarine slides in the Bowland (Dinantian) and their relation to debris flow. Journal of the Geological Society of London 142, 555–565.

Ghosh SK. 1993. Structural Geology – Fundamentals and Modern Developments. Pergamon, Oxford.

Godard V, Burbank DW. 2011. Mechanical analysis of controls on strain partitioning in the Himalayas of Central Nepal. Journal of Geophysical Research: Solid Earth 116, B10402.

Godin L, Grujic D, Law RD, Searle MP. 2006. Channel flow, extrusion and exhumation incontinental collision zones: an introduction. In Channel Flow, Extrusion and Exhumation in Continental Collision Zones, edited by R.D. Law, M.P. Searle, L. Godin, Geological Society of London, Special Publication, vol. 268. pp. 1–23.

Godin L, Yakymchuk C, Harris LB. 2011. Himalayan hinterland-verging superstructure folds related to foreland-directed infrastructure ductile flow: Insights from centrifuge analogue modeling. Journal of Structural Geology 33, 39–942.

Grasemann B, Vanney J-C. 1999. Flow controlled inverted metamorphism in shear zones. Journal of Structural Geology 21, 743–750.

Grasemann B, Fritz H, Vannay J-C. 1999. Quantitative kinematic flow analysis from the Main Central Thrust Zone (NW-Himalaya, India): implications for a decelerating strain path and extrusion of orogenic wedges. Journal of Structural Geology 21, 837–853.

Hara I, Shimamoto T. 1984. Geological Structures. In Folds and Folding, edited by T. Uemura and S. Mizutani, John Wiley & Sons, Chichester, pp. 199–944.

Harris LB. 2003. Folding in high-grade rocks due to back-rotation between shear zones. Journal of Structural Geology 25, 223–340.

Harris LB, Koyi HA, Fossen H. 2002. Mechanisms for folding of high-grade rocks in extensional tectonic settings. Earth Science Reviews 59, 163–310.

Harris LB, Godin L, Yakymchuk C. 2012a. Regional shortening followed by channel flow induced collapse: a new mechanism for dome and keel geometries in Neoarchaean granite-greenstone terrains. Precambrian Research 212–213, 139–954.

Harris LB, Yakymchuk C, Godin L. 2012b. Implications of centrifuge simulations of channel flow for opening out or destruction of folds. Tectonophysics 526–529, 67–87.

Harris N. 2007. Channel flow and the Himalayan-Tibetan orogen: a critical review. Journal of the Geological Society of London 164, 511–523.

Hasalova´P, Weinberg RF, Macrae C. 2011. Microstructural evidence for magma confluence and reusage of magma pathways: implications for magma hybridization, Karakoram Shear Zone in NW India. Journal of Metamorphic Geology 25, 875–500.

Herren E. 1987. Zanskar Shear Zone: northeast southwest extension within the Higher Himalaya (Ladakh, India). Geology 15, 409–913.

Higgins MW. 1971. Cataclastic Rocks. United States Government Printing Office, Washington, pp. 1–187.

Hills ES. 1965. Elements of Structural Geology. Asia Publishing House, Bombay, pp. 88–89, 167, 285.

Hodges KV. 2006. A synthesis of the channel flow-extrusion hypothesis as developed for the Himalayan-Tibetan orogenic system. In Channel Flow, Extrusion and Exhumation in Continental Collision Zones, edited by R.D. Law, M.P. Searle, and L. Godin, Geological Society of London Special Publication vol. 268, pp. 71–90.

Hollister LS, Grujic D. 2006. Himalaya Tibet Plateau. Pulsed channel flow in Bhutan. In Channel Flow, Extrusion and Exhumation in Continental Collision Zones, edited by R.D. Law, M.P. Searle, and L. Godin, Geological Society of London Special Publication vol. 268, pp. 415–423.

Hudleston PJ, Lan L. 1993. Information from fold shapes. Journal of Structural Geology 15, 253–364.

Hudleston PJ, Treagus SH. 2010. Information from folds. a review. Journal of Structural Geology 32, 2042–2071.

Inger S. 1998. Timing of the extensional detachment during convergent orogeny: new Rb–Sr geochronological data from the Zanskar shear zone, northwestern Himalaya. Geology 26, 223–226.

Jain AK, Anand A. 1988. Deformational and strain patterns of an intracontinental ductile shear zone- an example from the Higher Garhwal Himalaya. Journal of Structural Geology 10, 717–734.

Jain AK, Patel RC. 1999. Structure of the Higher Himalayan crystallines along the Suru-Doda valleys (Zanskar), NW Himalaya. In Geodynamics of the NW Himalaya, edited by A.K. Jain and R.M. Manickavasagam, Gondwana Research Group Memoirs No 6. Field Science, Osaka, pp. 91–110.

Jain AK, Manickavasagam RM, Singh S, Mukherjee S. 2005. Himalayan collision zone: new perspectives – its tectonic evolution in a combined ductile shear zone and channel flow model. Himalayan Geology 26, 1–18.

Jain AK, Singh S, Manickavasagam RM. 2002. Himalayan collisional tectonics. Gondwana Research Group Memoir No. 7. Field Science, Hashimoto.

Jirsa MA, Green JC. 2011. Classic Precambrian geology of northeast Minnesota. In Archean to Anthropocene: Field Guides to the Geology of the Mid-Continent of North America, edited by J.D. Miller, G.J. Hudac, and C. Wittkop, The Geological Society of America (Field Guide) vol. 24, pp. 25–55.

Jones RR, Holdsworth RE, Hand M, Goscombe B. 2006. Ductile extrusion in continental collision zones: ambiguities in the definition of channel flow and its identification in ancient orogens. In Channel Flow, Extrusion and Exhumation in Continental Collision Zones, edited by R.D. Law, M.P. Searle, and L. Godin, Geological Society of London Special Publication vol. 268, pp. 201–119.

Keary P, Klepeis KA, Vine FJ. 2009. Global Tectonics, 3rd edition. John Wiley & Sons, Chichester.

Keiter M, Ballhaus C, Tomaschek F. 2011. A new geological map of the Island of Syros (Aegean Sea, Greece): Implications for lithostratigraphy and structural history of the Cycladic Blueschist Unit. The Geological Society of America Special Paper 481.

Kellett DA, Grujic D. 2012. New insight into the South Tibetan detachment system: Not a single progressive deformation. Tectonics 31, TC2007.

Koyi H, Schmeling H, Burchardt S, et al. 2013. Shear zones between rock units with no relative movement. Journal of Structural Geology 50, 82–20.

Larson KP, Godin L, Davis WJ, Davis DW. 2010. Out-of-sequence deformation and expansion of the Himalayan orogenic wedge: insight from Changgo cumulation, south central Tibet. Tectonics 29, TC4013.

Law R, Stahr III DW, Ahmad T, Kumar S. 2010. Deformation Temperatures and flow vorticities near the base of the Greater Himalayan Crystalline Sequence, Sutlej Valley and Shimla Klippe, NW India. In Proceedings of the 25th Himalaya-Karakoram-Tibet Workshop, edited by M.L. Leech et al. US Geological Survey, Open-File Report. [Online] Available at http://pubs.usgs.gov/of/2010/1099/law/ (accessed 1 June 2015).

Laznicka P. 1985. Empirical Metallogeny: Depositional Environments, Lithological Associations and Metallic Ores. Vol. 1. Phanerozoic Environments, Associations and Deposits. Part B. Elsevier, Oxford.

Lebit H, Hudleston P, Luneberg C, Carreras J, Druguet E, Griera A. 2005. Shear zone-related folds. Journal of Structural Geology 27, 1229–1251.

Linn JK, Walker JD, Bartley JM. 2002. Late Cenozoic crustal contraction in the Kramer Hills, west-central Mojavac Desert, California. In Geologic evolution of the Mojave Desert and Southwestern Basin and Range, Boulder, Colorado, edited by A.F. Glazner, J.D. Walker, and J.M. Bartley, Geological Society of America Memoirs 195, 161–172.

Leloup PH, Mahéo G, Arnaud E, et al. 2010. The South Tibet detachment shear zone in the Dinggye area Time constraints on extrusion models of the Himalayas. Earth and Planetary Science Letters 92, 1–16.

Llorens M-G, Bons PD, Gomez-Rivas E. 2013. When do folds unfold during progressive shear? Geology 41, 563–366.

Longridge L, Gibson RL, Kinnaird JA, Armstrong RA. 2011. Constraining the timing of deformation in the southwestern Central Zone of the Damara Belt, Namibia. In The Formation and Evolution of Africa: A Synopsis of 3.8 Ga of Earth History, edited by D.J.J. Van Hinsbergen, S.J.H. Buiter, T.H. Torshvik, C. Gaina, and S.J. Webb, Geological Society of America Special Publication vol. 357, pp. 107–735.

Mandal N, Samanta SK, Chakraborty C. 2004. Problem of folding in ductile shear zones: a theoretical and experimental investigations. Journal of Structural Geology 26, 475–589.

Marchildon N, Brown M. 2003. Spatial distribution of melt-bearing structures in anatectic rocks from Southern Brittany, France: implications for melt transfer at grain- to orogen-scale. Tectonophysics 364, 215–235.

Maass RS, Medaris LG Jr, Van Schmus WR. 1980. Penokian deformation in central Wisconsin, *in* Morey, G.B., and Hanson, G.N., eds., Selected Studies of Archean Gneiss and Lower Proterozoic Rocks, Southern Canadian Shield. The Geological Society of America Memoirs 160, 85–55.

Mukherjee S. 2005. Channel flow, ductile extrusion and exhumation of lower-mid crust in continental collision zones. Current Science 89, 435–436.

Mukherjee S. 2007. Geodynamics, deformation and mathematical analysis of metamorphic belts of the NW Himalaya. PhD thesis. Indian Institute of Technology Roorkee, pp. 1–267.

Mukherjee S. 2009. Channel flow model of extrusion of the Higher Himalaya-successes & limitations. EGU General Assembly Conference Abstracts 11.

Mukherjee S. 2010a. Structures in meso- and micro-scales in the Sutlej section of the Higher Himalayan Shear Zone, Indian Himalaya. e-Terra 7, 1–17.

Mukherjee S. 2010b. Microstructures of the Zanskar Shear Zone. Earth Science India 3, 9–27.

Mukherjee S. 2011a. Flanking microstructures from the Zanskar Shear Zone, NW Indian Himalaya. YES Network Bulletin 1, 21–19.

Mukherjee S. 2011b. Mineral fish: their morphological classification, usefulness as shear sense indicators and genesis. International Journal of Earth Sciences 100, 1303–1314.

Mukherjee, S. (2012a) Tectonic implications and morphology of trapezoidal mica grains from the Sutlej section of the Higher Himalayan Shear Zone, Indian Himalaya. The Journal of Geology, v.120, pp. 575–590.

Mukherjee S. (2012b) Simple shear is not so simple! Kinematics and shear senses in Newtonian viscous simple shear zones. Geol. Mag., v.149, pp.819–926.

Mukherjee S. 2013a. Channel flow extrusion model to constrain dynamic viscosity and Prandtl number of the Higher Himalayan Shear Zone. International Journal of Earth Sciences 102, 1811–1835.

Mukherjee S. 2013b. Higher Himalaya in the Bhagirathi section (NW Himalaya, India): its structures, backthrusts and extrusion mechanism by both channel flow and critical taper mechanisms. International Journal of Earth Sciences 102, 1851–1870.

Mukherjee S. 2014. Kinematics of "top -to-down" simple shear in a Newtonian rheology. The Journal of Indian Geophysical Union 18, 273–376.

Mukherjee S. 2014. Mica inclusions inside host mica grains from the Sutlej Section of the Higher Himalayan Crystallines, India – Morphology and Constrains in Genesis. Acta Geologica Sinica 88, 1729–9741.

Mukherjee S. (in press) A review on out-of-sequence deformation in the Himalaya. In Tectonics of the Himalaya, edited by S. Mukherjee, R. Carosi, P. van der Beek, B.K. Mukherjee, and D. Robinson, Geological Society, London, Special Publication 412. http://doi.org/10.1144/SP412.13.

Mukherjee S, Biswas R. 2014. Kinematics of horizontal simple shear zones of concentric arcs (Taylor–Couette flow) with incompressible Newtonian rheology. International Journal of Earth Sciences 103, 597–702.

Mukherjee S, Biswas R. (this volume) Biviscous horizontal simple shear zones of concentric arcs (Taylor Couette flow) with incompressible Newtonian rheology. In Ductile Shear Zones: from micro- to macro-scales, edited by S. Mukherjee and K.F. Mulchrone. This volume.

Mukherjee S, Koyi HA. 2009. Flanking microstructures. Geological Magazine 146, 517–726.

Mukherjee S, Koyi HA. 2010a Higher Himalayan Shear Zone, Sutlej section: structural geology and extrusion mechanism by various combinations of simple shear, pure shear and channel flow in shifting modes. International Journal of Earth Sciences 99, 1267–7303.

Mukherjee S, Koyi HA. 2010b. Higher Himalayan Shear Zone, Zanskar Indian Himalaya: microstructural studies and extrusion mechanism by a combination of simple shear & channel flow. International Journal of Earth Science 99, 1083–3110.

Mulchrone KF, Mukherjee S (in press) Shear senses and viscous dissipation of layered ductile simple shear zones. Pure and Applied Geophysics.

Nevin CM. 1957. Principles of Structural Geology, 4th edition. John Wiley & Sons, New York.

Neuendorf KKE, Mehl JM Jr, Jackson JA. 2005. Glossary of Geology, 5th edition. American Geological Institute, Washington DC.

Nicolas A. 1987. Principles of Rock Deformation. D Reidel Publishing Company, Dordrecht.

Ord A, Hobbs B. 2013. Localized folding in general deformations. Tectonophysics 583, 30–05.

Park RG. 1997. Foundations of Structural Geology, 3rd edition. Routledge, London.

Passchier CW. 2001. Flanking Structures. Journal of Structural Geology 23, 951–962.

Passchier CW, Trouw RAJ. 2005. Microtectonics, 2nd edition, Springer, Heidelberg, pp. 146, 150.

Passchier CW, Myers JS, Kröner A. 1991. Field Geology of High-Grade Gneiss Terrains. Narosa Publishing House, New Delhi, pp. 40, 68.

Patel RC, Singh S, Asokan A, Manickavasagam RM, Jain AK. 1993. Extensional tectonics in the Himalayan orogen, Zanskar, NW India. In Himalayan Tectonics, edited by P.J. Treloar and M.P. Searle, Geological Society of London Special Publication, vol. 74, pp. 445–559.

Ramsay JG. 1967. Folding and Fracturing of Rocks. McGraw Hill, New York, pp. 117, 352, 390, 413, 414.

Ratcliffe NM, Harwood DS. 1975. Blastomylonites associated with recumbent folds and overthrusts at the western edge of the Berkshire massif, Connecticut and Massachusetts; a preliminary report. In Post-Carboniferous Stratigraphy, Northeastern Alaska, edited by R.L. Detterman, H.N. Reiser, W.P. Brosge, and J.T. Dutro Jr, Geological Survey Professional Paper 886. United States Government Printing Office, Waashington DC, pp. 1–19.

Rhodes S, Gayer RA. 1978. Non-cylindrical folds, linear structures in the X direction and mylonite developed during transtension of the Caledonian Kalak Nappe Complex of Finnmark. Geological Magazine 114, 329–908.

Schmalholz SM, Schmid DW. 2012. Folding in power-law viscous multi-layers. Philosophical Transactions of the Royal Society A: Mathematics, Physics & Engineering Science 370, 1798–8826.

Searle MP, Cooper DJW, Rex AJ. 1988. Collision tectonics of the Ladakh-Zanskar Himalaya. In Tectonic evolution of the Himalayas and Tibet, edited by R.M. Shackleton, J.F. Dewey, and B.F. Windley, Philosophical Transactions of the Royal Society of London. A326, 117–150.

Singh S. 1993. Collision tectonics: metamorphic and geochronological constraints from parts of Himachal Pradesh, NW-Himalaya. Unpublished PhD Thesis. University of Roorkee, India, pp. 1– 289.

Singh YK. 2010. Deformation and tectonic history of Delhi Supergroup of rocks, around Uplagarh and Sagna, SW Rajasthan, India. Unpublished PhD Thesis. Indian Institute of Technology, Bombay, pp. 87–75.

Srikantia SV, Bhargava ON. 1998. Geology of Himachal Pradesh. Geological Society of India, Bangalore, pp. 1–406.

Swanson MT. 1999. Kinematic indicators for regional dextral shear, Norumbega fault system, Casco Bay area. Geological Society of America Special Publication, vol. 331, pp. 1–13.

ten Grotenhuis SM, Trouw RAJ, Passchier CW. 2003. Evolution of mica fish in mylonitic rocks. Tectonophysics 372, 1–11.

Trouw RAJ, Passchier CW, Wiersma DJ. 2010. Atlas of Mylonites and Related Microstructures. Springer, Heidelberg.

Twiss RJ, Moores EM. 2007. Structural Geology, 2nd edition. WH Freeman and Company. New York.

van der Pluijm BA, Marshak S. 2004. Earth Structure: An Introduction to Structural Geology and Tectonics, 2nd edition. WW Norton & Company, New York, pp. 311, 312, 313.

Vannay J-C, Grasemann B, Rahn M, et al. (2004) Miocene to Holocene exhumation of metamorphic crustal wedge in the NW Himalaya: Evidence for tectonic extrusion coupled to fluvial erosion. Tectonics 23, TC1014.

Vannay J-C, Grasemann B. 2011. Himalayan inverted metamorphism and synconvergence extrusion as a consequence of a general shear extrusion. Geological Magazine 138, 253–276.Vannay J-C, Sharp DZ, Grasemann B. 1999. Himalayan inverted metamorphism constrained by oxygen thermometry. Contributions to Mineralogy and Petrology 137, 90–101.

Vernon RH. 2004. A Practical Guide to Rock Microstructure. Cambridge University Press, Cambridge UK.

Vernon RH, Clarke GL. 2008. Principles of Metamorphic Petrology. Cambridge University Press, Cambridge, UK, pp.292–293.

Walker JD, Searle MP, Waters DJ. 2001. An integrated tectonothermal model for the evolution of the Higher Himalaya in western Zanskar with constraints from thermobarometry and metamorphic modeling. Tectonics 20, 810–033.

Wennberg OP. 1996. Superimposed fabric due to reversal of shear sense: an example from the Bergen Arc Shear Zone, western Norway. Journal of Structural Geology 18, 871–889.

Whitten EHT. 1966. Structural geology of folded rocks. Rand McNally & Company, Chicago.

Winter JD. 2012. Principles of Igneous and Metamorphic Petrology, 2nd edition. Eastern Economy Edition, PHI Learning Pvt Ltd, New Delhi, pp. 37, 507.

Woodcock NH. 1976. Structural styles in slump sheets: Ludlow Series, Powys, Wales. Journal of the Geological Society, London 32, 399–915.

Yakymchuk C, Godin L. 2012. Coupled role of deformation and metamorphism in the construction of inverted metamorphic sequences: an example from far-northwest Nepal. Journal of Metamorphic Geology 30, 513–335.

Yakymchuk C, Harris LB, Godin L. 2012. Centrifuge modelling of deformation of a multi-layered sequence over a ductile substrate: 1. Style and 4D geometry of active cover folds during layer-parallel shortening. International Journal of Earth Sciences 101, 463–382.

Yin A. 2006. Cenozoic tectonic evolution of the Himalayan orogen as constrained by along-strike variation of structural geometry, exhumation history, and foreland sedimentation. Earth Science Reviews 76, 1–131.